

THE GREEN SYNTHESIS AND EVALUATION
OF SILVER NANOPARTICLES AND
ZINC OXIDE NANOPARTICLES

BY

BELLSABEL GEBEAR-EIGZABHER

A THESIS

Submitted in partial fulfilment of the requirements
For the degree of Doctor of Philosophy in the
Applied Chemistry Graduate Program of
Delaware State University

Dover, Delaware
December, 2017

This thesis is approved by the following members of the Final Oral Review Committee:

Dr. Daniela Radu, Committee Chairperson, Department of Chemistry, Delaware State University

Dr. Aristides Marcano, Committee Member, Department of Physics and Engineering, Delaware State University

Dr. Cherese Winstead-Casson, Committee Member, Department of Chemistry, Delaware State University

Dr. Bizuneh Workie, Committee Member, Department of Chemistry, Delaware State University

Dr. Sidney Katz, Committee Member, Department of Chemistry, Rutgers University

DEDICATION

To God

"If I have seen further, it is by standing on the shoulders of giants."-Sir Isaac Newton

I dedicate this thesis to my parents,
Hailekiros Gebreegziabher and Alemishet Kidane.

My sister, Meron Hailekiros,
and all of my friends.

ACKNOWLEDGEMENT

I would like to start by thanking God. It is only through the grace of God that I had the strength to complete my thesis. I would like to thank my parents, Alemishet Kidane and Hailekiros Gebreegziabher, for their limitless love and support.

I thank Dr. Daniela Radu, Department of Chemistry for the microscopy training, advisement and help during the time of my work. I could not have imagined having a better advisor and mentor for my Ph.D. She is one of the most brilliant scientists I have ever met, and I am extremely grateful to have her as an advisor. I appreciate becoming a Ph.D. student in her laboratory and am thankful for her continuous support. Dr. Radu gave me the encouragement to be successful and independent in the laboratory. She was willing to direct me to specific reading materials, and her leadership was invaluable. She is always available for her students, professional, and a pillar of strength and wisdom. I was privileged and honored to have her as the Chair of my Thesis Committee.

I would genuinely like to thank my graduate school professor at Rutgers University-Camden, Dr. Sidney Katz for being a part of my accomplishment. His suggestions, comments, and wisdom benefited me so much and he has been supportive and helpful since day one.

I also want to thank Dr. Aristides Marcano, Department of Physics and Engineering. I am very thankful to work under him as a student. He is an inspiring professor, cheerful and motivating, and always available to help. The professional help I really enjoyed learning quantum mechanics from Dr. Marcano. His passion for optics is inspiring, and the support in my research and education will last me a lifetime.

I want to thank Dr. Cherese Winstead-Casson, Chairperson of the Chemistry Department for being an amazing mentor, having patience, and a refreshing sense of humor. Meeting her and

having her as a professor taught me how to teach and I realize what a huge responsibility education is. She has been instrumental in achieving my academic goal.

Additionally, I thank Dr. Bizuneh Workie. I thank him for his incredible help throughout the years. His belief in my future success has kept me focused. From the bottom of my heart, I appreciate it.

I would like to also thank Dr. Clytrice Watson, former Dean of the CMNST. I greatly appreciate her generosity. Dr. Watson changed the way I view the world and my place in it. I wish to thank my friends, mentors, professors, classmates and lab mates for their help. I would also like to express my heartfelt gratitude to Dr. Charlie Wilson, Dean of CMNST the administration and the graduate school for offering me their full support when I needed it. Without the financial support of the graduate school, this work would not have been possible.

THE GREEN SYNTHESIS AND EVALUATION OF SILVER NANOPARTICLES AND ZINC OXIDE NANOPARTICLES

Bellsabel Gebear-Eigzabher

Faculty Advisor: Dr. Daniela Radu

ABSTRACT

Nanoparticle (NP) research has received exceptional attention as the field of study that contributes to transforming the world of materials science. When implementing NPs in consumer and industrial products, their unique properties improve technologies to the extent of significant game-changing breakthroughs. Conversely, the increased production of NPs, their use, their disposal or inadvertent release in the environment drove the need for processes and policies that ensures consumer and environmental safety. Mitigation of any harmful effects that NPs could potentially have combines methods of safe preparation, safe handling and safe disposal as well as containment of any inadvertent release. Our focus is in safe preparation of nanomaterials and we report green and energy efficient synthesis methods for metal NPs and metal oxide NPs of two popular materials: silver (Ag) and zinc oxide (ZnO).

The thesis explained: 1) The impact of NPs in nowadays' world; 2) Synthesis methods that were designed to include environmentally-friendly starting materials and energy-saving fabrication processes, with emphasis on maintaining NPs final size and morphology when compared with existing methods; and 3) Nanoparticles characterization and data collection which allowed us to determine and/or validate their properties.

Nanoparticles were studied using transmission electron microscope (TEM), X-Ray powder diffraction (XRD), low-voltage (5 keV) transmission electron microscopy (LV EM 5), Fourier-Transform Infrared Spectroscopy (FT-IR), and Ultraviolet-Visible (UV-Vis) spectroscopy.

We developed an aqueous-based preparation of zinc oxide nanoparticles (ZnO NPs) using microwave-assisted chemistry to render a well-controlled particle size distribution within each set of reaction conditions in the range of 15 nm to 75 nm.

We developed a scalable silver nanoparticles synthesis by chemical reduction methods. The NPs could be used in consumer products. The measurement tools for consumer products were also used on in-house synthesized Ag NPs.

Commercially available silver nanoparticles have been compared with the in-house synthesized ones and characterized by Photothermal Lens (PTL) Spectroscopy. In respect to particle size and morphology, the Ag NPs synthesized by chemical reduction methods are similar to Ag nanoparticle solution available in the market. However, the synthesized nanoparticles are high in concentration and do not show signs of aggregation or agglomeration. It was concluded that our Ag NPs are superior to the commercially available ones by exhibiting large concentrations in ultra-stable dispersions.

TABLE OF CONTENTS

LIST OF TABLES	x
LIST OF FIGURES	xi
LIST OF ABBRIVATIONS	xiii
1. CHAPTER 1. INTRODUCCION.....	1
1.1 Impact of Nanomaterials	2
2. CHAPTER 2. LITERATURE REVIEW	5
2.1 Nanomaterial and Global Sustainability	5
2.1.1 Applications of Nanomaterials: Energy Storage	6
2.1.2 Applications of Nanomaterials: Agriculture	7
2.2 Nanoparticle Synthesis	7
2.2.1 Precipitation for Nanoparticle Synthesis	8
2.2.2 Nucleation	10
2.2.3 Growth.....	11
2.2.4 Ostwald Ripening	12
2.2.5 Chemical Reduction in Synthesis of Metallic Nanoparticles	13
2.2.6 Microwave Precipitation	15
2.2.7 Sol-Gel Chemistry	16
2.2.8 Pechini Method	17
2.2.9 Microemulsion	17

2.2.10 Hydrothermal / Solvothermal Nanoparticles Synthesis	18
2.2.11 Biomimetic Synthesis.....	19
2.3 Nanofluid.....	20
2.3.1 Nanofluid Materials.....	20
2.4 Materials Characterization	21
2.4.1 Transmission Electron Microscopy.....	21
2.4.2 Electron Microscopy for Analysis of Nanoparticles	22
2.4.3 Morphological Information Acquired With TEM.....	22
2.4.4 Developments of TEM.....	23
2.4.5 Low Voltage Electron Microscopy	23
2.4.6 Low Voltage Electron Microscope 5 kV (LVEM5).....	24
2.4.7 Nanomaterials Visualization	25
2.4.8 Sample Preparation	26
2.4.9 Side-Effects of TEM Grids	26
2.4.10 Conclusion.....	27
3. CHAPTER 3. EXPERIMENTAL	29
3.1 Materials.....	29
3.2 Instrumentation.....	30
3.3 Characterization Methods	37
3.4 Synthesis of Zinc Oxide	40

3.5 Synthesis of Silver.....	42
3.6 Fabrication of In-House Synthesized Silver Inks.....	44
3.7 Fabrication of In-House Synthesized Silver Films	44
4. CHAPTER 4. RESULTS AND DISCUSSION.....	47
4.1 Characterization of Synthesized Zinc Oxide Nanoparticle	47
4.2 Characterization of In-House Synthesized Silver Nanoparticle.....	54
4.3 Characterization of Commercially Available Silver Nanoparticle	61
5. CHAPTER 5. CONCLUSION.....	65
5.1 Summary of Research Findings of Zinc Oxide Nanoparticle	65
5.1.1 Summary of Research Findings of Synthesized Silver Nanoparticle	66
5.1.2 Summary of Research Findings of Commercially Available Silver	66
5.2 Final Conclusions.....	67
5.2.1 Zinc Oxide Nanoparticles Synthesis	67
5.2.2 Synthesized Silver Nanoparticles Synthesis	67
5.3 Discussion	69
5.3.1 Discussion of Zinc Oxide Nanoparticles.....	69
5.3.2 Discussion of Synthesized Silver Nanoparticles.....	69
5.4 Suggestion for Future Research	70
5.5 Technological Applications of ZnO and Ag Nanoparticles	70
REFERENCES.....	75

LIST OF TABLES

Table 1. Properties of Zinc Oxide Synthesized in Our Lab 47

Table 2. Batch Synthesis Overview 55

LIST OF FIGURES

Figure 1. Schematic Representation of Solvothermal Synthesis of Nanoparticles.....	11
Figure 2. Growth of Silver Nanoparticle Synthesis	11
Figure 3. Ostwald Ripening: Large Particles Grow at The Expense of Smaller Particles.....	12
Figure 4. Sol-gel Preparation of Nanomaterials.....	16
Figure 5. Diagram of Schulman's Microemulsion Model	18
Figure 6. Size Comparison of Typical TEM and LVEM5 TEM	30
Figure 7. Schematic Diagram for PTL Experiment	35
Figure 8. Conventional VS Microwave Heating.....	36
Figure 9. TEM Grid	38
Figure 10. Schematic of Zinc Oxide Nanoparticle Microwave Assisted Synthesis	41
Figure 11. Schematic of In-House Synthesized Silver Nanoparticle Synthesis	43
Figure 12. Collected Reaction Mixture (Wet Pellet)	43
Figure 13. One Layer Spray Coating of Ag Sample Ink 1 (a) Plasma Treated (b) Without Plasma Treatment	46
Figure 14. One Layer Spray Coating of Ag (a) & (b) Sample Ink 1 (c) Spin Coating of Sample Ink 2	46
Figure 15. XRD of Zinc Oxide (a) Sample ZnO 1 (b) Sample ZnO 3 (c) JCPDS Reference	49
Figure 16. (a) TEM of ZnO Sample 1 (b) Particle Size Distribution Histogram of ZnO Sample 1 (c) TEM of ZnO Sample 3 (d) TEM ZnO Sample 4.....	50
Figure 17. LVEM5 Images of Zinc Oxide Nanoparticles Taken at ~5kV in TEM mode (a) Conventional Synthesis of Zinc Oxide (b) Particle Size Distribution of The Conventionally	

Synthesized Zinc Oxide Nanoparticles (c) Microwave-Assisted Synthesis at 5 min (d) Sample 1 Histogram.....	51
Figure 18. UV-Vis Absorption Spectra of Zinc Oxide	52
Figure 19. FT-IR of Zinc Oxide Nanoparticles.....	53
Figure 20. In-House Synthesized Silver Nanoparticles Growth Mechanism	54
Figure 21. HRTEM of Synthesized Silver Nanoparticles (a) Sample Ag 1(b) Sample Ag2 (c) Sample Ag 3 (d) Sample Ag 4 (e) Sample Ag 5 and (f) Sample Ag 6	57
Figure 22. (a) Low Voltage SEM Sample Ag 1 (b) SEM Sample Ag 1 At Lower Magnification	58
Figure 23. (a) Absorbance of Synthesized Silver Nanoparticles (b) Absorbance of Silver Nanoparticles as A Function of Concentration.....	59
Figure 24. Nanocomposix Colloidal Solutions of Various Silver Nanoparticle Size	61
Figure 25. UV-Vis Absorbance of Nanocomposix Nanoparticles as A Function of Size	62
Figure 26. HRTEM of Nanocomposix Silver Nanoparticles (Used with permission from Nanocomposix [170])	62
Figure 27. PTL Spectra of Nanocomposix Nanoparticles	63

LIST OF ABBRIVATIONS

2D	Two-dimensional
3D	Three-dimensional
4D	Fourth-dimension
AOT	Aerosol OT
ATR	Attenuated total reflectance
CCD	Charged-coupled device
CTAB	Centrimonium bromide
CW	Continuous wave
DFT	Density functional theory
DMF	N,N-dimethylformamide
EM	Electron microscope
ETEM	Environmental transmission electron microscope
FCC	Face centered cube
FT-IR	Fourier transform infrared spectroscopy
HR-TEM	High resolution transmission electron microscope
IR	Infrared spectroscopy

JCPDS	Joint committee on Powder diffraction standards
LED	Light emitting diode
LVEM5	Low voltage electron microscope 5 kV
NMR	Nuclear magnetic resonance
MTP	Multiple twinned particles
NP	Nanoparticle
PED	Precession electron diffraction
PSD	Particle size distribution
PTL	Photothermal lens spectroscopy
PVA	Poly(vinyl alcohol)
RF	Radio frequency
RFID	Radio frequency identification
RPM	Rotations per minute
SEM	Scanning electron microscope
SWCNT	Single walled carbon nanotubes
STEM	Scanning transmission electron microscope
TADDD	bis(11-trimethylammoniumdecanoylaminoethyl) disulfide dibromide

TEM	Transmission electron microscope
UV-Vis	Ultraviolet visible spectroscopy
XRD	X-ray diffraction

CHAPTER 1. INTRODUCCION

Background

Nanomaterials, a class of materials with at least one geometric dimension below 100 nm, contribute to a plethora of industrial applications such as electronics, catalysis, the biomedical field, cosmetics, and more. Nanoparticles in electronic applications include solar absorbers and solar cells, radio frequency identification (RFID) tags, light emitting diodes (LED) [1]. These applications are essential to the progress of our technology-driven society and are motivating the research to elaborate various synthetic and processing methodologies. It is critical, however, that the production of these useful materials is green and energy efficient. Our focus on establishing environmentally friendly, simple preparation and purification procedures to fabricate ubiquitous nanomaterials such as metal and metal oxide nanoparticles motivated the need to deliver proof-of-concept models for future endeavors in this field. As examples, replacement of harmful solvents used in nanoparticles synthesis with water, use of energy saving microwave-assisted synthesis, and a careful selection of starting materials are part of the thesis focus.

Two representatives of each class of materials were chosen for the demonstration of benign methods in nanomaterials fabrication. Of critical importance are the properties of these materials in regard to their particle size, particle size distribution, structural, and functional properties (optical and electrical).

In this line, high-throughput methods to determine nanoparticles properties are desired, toward gaining fast insight over the usefulness of the materials in replacing their counterparts obtained through current processes.

The several techniques employed in characterizing the nanoparticles synthesized by our approach are as follows. X-Ray powder diffraction (XRD) to determine nanomaterials crystal structure, low-voltage transmission electron microscopy (TEM) to evaluate nanoparticle size and particle size distribution, Fourier-Transform Infrared Spectroscopy (FT-IR) to obtain information on organic materials present on the nanoparticles surface and Ultraviolet-Visible (UV-Vis) spectroscopy to validate optical properties.

1.1 Impact of Nanomaterials

Nanoparticles demonstrated impact in energy related applications will lead to decrease the use of fossil fuels and contribute to mitigating climate change effects. To further add to the environmental dimension of this impact, it is important that the synthesis, use and disposal of nanomaterials is well understood. Synthesizing and implementing environmentally benign nanomaterials is a long-term challenge and requires a collaborative effort from chemists and chemical engineers, materials scientists, biomedical scientists, environmental scientist and policy makers, to name a few. Given the high reactivity of nanomaterials, their impact on environment needs to be evaluated and therefore, continuing development of characterization techniques, computational methods, and mechanistic studies of nanoparticle interaction with biological organisms is essential to the understanding long-term impact of nanoparticles on the environment.

To exemplify, global access to clean water may likely be determined by efficiently removing organic and inorganic compounds from polluted water and nanoparticles technologies could replace current remediation techniques. For instance, zero-valent iron may be used as a

reducing agent, and to change organic pollutants into benign forms. Using zero-valent iron in nanoparticle form would increase reaction rate; however, little is known in regard to any harmful effects of such nanoparticles if uptake in biological systems occurs. Additionally, sorbents for inorganic anions benefit from high surface area of metal and metal oxide nanomaterials [2,3]. In water remediation, nanoparticle composite oxides such as Fe_2O_3 , SiO_2 , and Al_2O_3 , have a high affinity for compounds of arsenic, with which water supplies in many parts of the world supply contaminated [2]. However, upon surface adsorption of the toxic species, nontoxic materials such as Fe_2O_3 nanoparticles could become toxic and due to size confinement, could cross into biological tissue. Such aspects need to be elucidated, and further processing of to mitigate and ultimately eliminate any side effects of nanomaterials used.

Recent advances in imaging, X-ray techniques, and optical methods have improved the ability to characterize the properties that most likely control interactions between nanoparticles and their surrounding medium.

Thesis Framework

The work is focused on the synthesis and characterization of zinc oxide and silver nanoparticles using sustainable, non-toxic materials and energy-saving synthetic methodologies. The properties of elemental silver nanoparticles and zinc oxide nanoparticles were evaluated using various analytical techniques such as microscopy and spectroscopy. Zinc oxide nanoparticles structural and optoelectronic characteristics were measured using XRD, FT-IR, TEM, and UV-Vis. The methods need to be used in combination because they complement each other to provide information about zinc oxide nanomaterial. The elemental silver nanoparticles

characterization included TEM, UV-Vis, and photothermal lens (PTL) spectrometry. An extensive PTL study was performed to compare the in-house nanoparticles with commercially available ones.

Chapter two provides the background and significance of the thesis in the context of currently reported efforts in the nanomaterials fields. This literature review emphasizes the importance of nanoparticle research and development.

Chapter three will discuss the experimental methods and advantages and disadvantages of the instrumental methods used to characterize the zinc oxide and silver nanoparticles.

Chapter four presents the results of synthetic and characterization work.

Chapter five includes concluding remarks and future research goals for sustainable nanotechnologies.

CHAPTER 2. LITERATURE REVIEW

2.1 Nanomaterial and Global Sustainability

In the last three decades, applications of nanomaterials and nanotechnology have transformed the field of chemistry [4,5]. According to the 1995 “Holy Grail” issue of *Accounts of Chemical Research*, upon their discovery, nanoparticles were synthesized in small amounts and studied out of curiosity. Thorough characterization of nanomaterials revealed their unique optoelectronic and catalytic properties and drove a large research effort toward synthesizing nanomaterials of different compositions, sizes, shapes and morphologies [6,7]. The motivation and challenge of chemistry are to manipulate and to exploit the capabilities of nanoparticle properties for discovering new functionalities and taking full advantage of their benign environmental effects while eliminating their adverse environmental impact.

As the extensive use of nanomaterials grew, the risk for inadvertent toxic release into the atmosphere and damaging the environment increased as well. Small amounts of nanomaterials pose less of a risk to the environment than nanomaterials produced in large quantities. Therefore, as the use of nanomaterials increases so does their potential to cause harm in the environment.

Consequently, the future of nanoparticles use in large amounts in emerging technologies will be determined by the potential for significant exposure during synthesis, use and disposal. The questions of how to predict nanomaterials’ impact on the environment and ensure that environmentally benign ways would be used for developing nano enabled technologies must be answered. Several applications which will require the use of nanomaterials in large quantities are presented as follows.

2.1.1 Applications of Nanomaterials: Energy Storage

The groundbreaking developments in portable electronics, and the urge to transform the automotive industry by introduction of electric cars prompted a fast-paced research/development in the area of energy storage, especially lithium-ion batteries.

The lithium-ion batteries using graphite and lithium cobalt oxide (LiCoO_2) are expensive and used in large amounts. Therefore, replacing Co with other inexpensive materials such as Fe, Ni, Al, and Mn, along with use of nanomaterials is perceived as reducing cost and increase performance.

Both the pros and cons of nanomaterials for lithium-ion batteries include allowing reactions that would not take place in bulk. The nanometer-size increases the frequency of insertion and removal in lithium-ion transport; furthermore, electron transport is also increased by the nanometer-size particles. The increased surface area of nanomaterials allows for high contact area therefore, increasing lithium-ion flux resulting in adjustable of electrode potentials.

The disadvantages of nanomaterials for lithium batteries include difficulty synthesizing controllable nanomaterials and the increased surface area that might permit side reactions [8].

In addition, electrical energy storage demands large amounts of materials, with the active cathode materials increasing the potential for toxic exposure to organisms during manufacturing, use, and disposal. Consequently, understanding the detrimental effects of these materials' impact on the environment and minimizing potential exposure is vital. Benign materials and methods of fabrication would be ultimately desired in using nanomaterials in energy storage.

2.1.2 Applications of Nanomaterials: Agriculture

The increased efficiency of agriculture toward a significant increase in food production is demanded by the global population increase. Given their potential to contribute to agricultural enhancements, in the next two decades, an increased use of nanomaterials in agriculture is expected [4]. The use of nanomaterials in food production would require large quantities of materials and will drive increased levels of potential nanoparticle exposure to animal and plant life. Early demonstration of increased effectiveness in fungicides and pesticides using Cu-based nanomaterials allowed further exploration of nanomaterials in such applications [9,10]. Recently, in an attempt to eliminate any side effects of nanoparticles, the use of polymer-based biodegradable nanoparticles to carry and deliver nutrients to the plant has emerged. Besides the biodegradability, polymeric nanomaterials allow easy functionalization to target specific delivery to specific location in plant. Such nanomaterials are expected to degrade under certain conditions such as light, heat, or pH to avoid soil accumulation and further uptake by non-targeted species.

Although nanoparticles have advantageous effects on crops, unfortunately, there is little understanding of the mechanism of nanoparticles action, to be able to evaluate potential long-term effects on soil and surrounding environments [9,10]. Elucidating these mechanistic approaches constitutes an active area of research which is expected to provide guidance for future use of nanoparticles in agriculture.

2.2 Nanoparticle Synthesis

The National Nanotechnology Initiative (<http://www.nano.gov>) focuses on the development of materials with at least one dimension ranging from 1 to 100 nm. This national strategic

research initiative developed the platform for a central understanding of the phenomena occurring at the nanoscale. Current applications and the future impact of nanotechnology ranging from its use in automotive to medicine, chemistry and earth sciences is outlined in Richard Feynman's 1959 speech at the California Institute of Technology (Caltech) titled, "There's Plenty of Room at the Bottom" [11].

Nanomaterials synthesis has seen significant growth in the past three decades. Several methodologies emerged, including: precipitation for nanoparticle synthesis, microwave precipitation, sol-gel chemistry, Pechini method, microemulsion, hydrothermal and solvothermal processing, templated syntheses, biomimetic syntheses. All these methodologies will be detailed as follows.

2.2.1 Precipitation for Nanoparticle Synthesis

Precipitation is a way of simultaneously separating compounds from an aqueous solution [12,13]. Precipitation involves nucleation, growth, coarsening and agglomeration to occur simultaneously [14–18]. Characteristics of precipitation reactions display the following steps, (Figure 1):

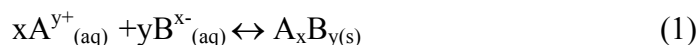
- (I) Supersaturation: Soluble species of precursor reagents reach high supersaturation;
- (II) Nucleation, which includes formation of nanoparticle nuclei at supersaturation;
- (III) Nanoparticles growth, involving nuclei growth until the precursors are fully consumed;

(IV) *Ostwald ripening*, involving further nanoparticle growth at the expense of smaller nanoparticles;

(V) *Saturation*, completing the nanoparticle formation.

To reach supersaturated fast, chemical reactants with low solubilities are selected.

The expression below summarizes the reaction to making the compound A_xB_y from ionic species, which often applies to nanoparticles synthesis: (all equations in chapter 2 are from reference [14])



Precipitation can also be prompted by chemical reduction, photoreduction, oxidations, and hydrolysis methods and induced by changing parameters such as temperature and concentration.

Products other than binary systems are more complicated because multiple species in ternary or quaternary systems must be precipitated simultaneously. **Figure 1** illustrates the first series of steps for nanoparticle formation known as nucleation. As precipitation begins, nucleation produces small crystals. However, they aggregate to form growing more stable particles. In the growth stage the nanoparticles grow until they have reached their final structure. This mechanism of nanoparticle formation in a solvothermal synthesis is a prominent example of the precipitation method. The mechanisms of nanoparticle formation explained below.

2.2.2 Nucleation

Nanoparticles formation involves two steps: nucleation and growth. In the nucleation step, the precursors are injected at high temperature and form until reaching a precursor saturation which results in forming nanoparticles nuclei. Further, the nuclei grow at the expense of the reaction precursors, until their full consumption.

To determine the degree of supersaturation (S) conditions the following equation below is necessary. K_{sp} represents the point at which the products and the reactants are balanced, and no more ions in solution can be formed or dissolved. The solubility, $S = C/C_{eq}$, where C and C_{eq} denote the concentrations of the solute at saturation and equilibrium. Therefore, the difference of the concentrations of the solute is represented by ΔC . The expression a_A and a_B represent the activities of the solution and are explained below [17].

$$S = \frac{a_A a_B}{K_{SP}} \quad (2)$$

When nucleation begins an equilibrium critical radius, R^* is determined and will continue to grow with $R > R^*$ and dissolve with $R < R^*$. R^* is expressed as

$$R^* = \frac{\alpha}{\Delta C} \quad (3)$$

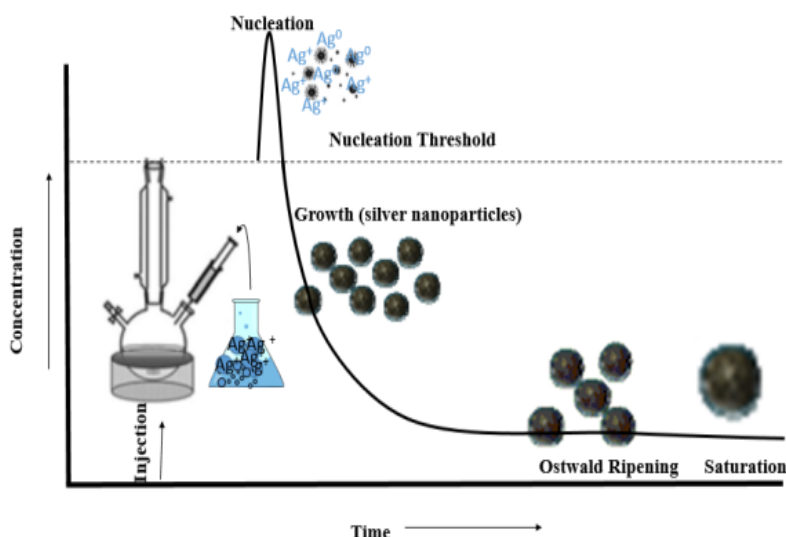


Figure 1. Schematic Representation of Solvothermal Synthesis of

2.2.3 Growth

Figure 2 explains the process of nanoparticle growth, which is controlled by reactions on the surface and diffusion of monomers to the surface. Experimental evidence implies that generally, precipitation reactions are diffusion-limited rather than reaction-limited [14].

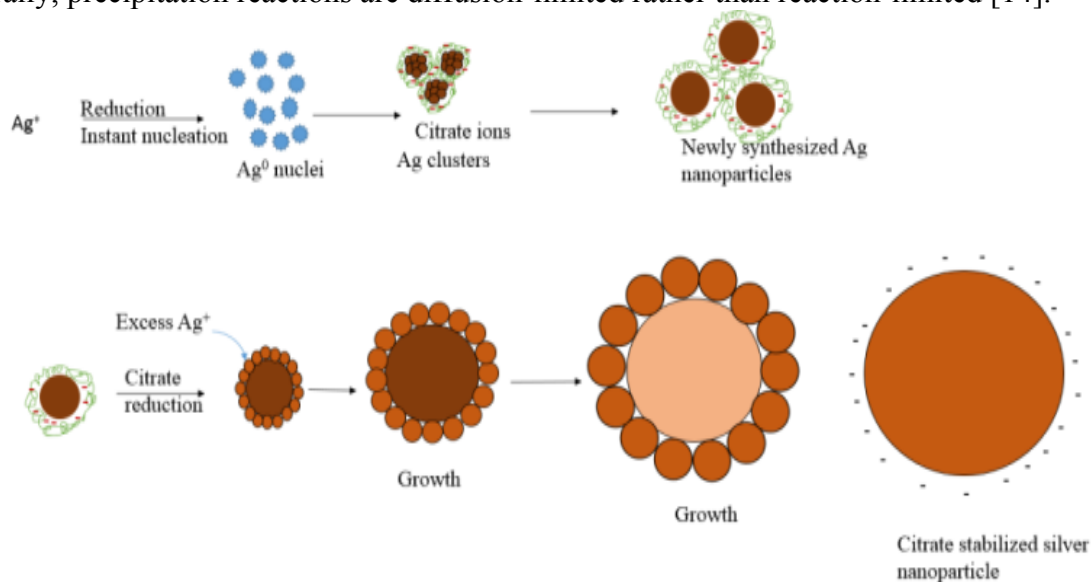


Figure 2. Growth of Silver Nanoparticle Synthesis

Therefore, major influences that determined the growth rate of nanoparticles include temperature and concentration of new material supplied. During growth, the reduction by citrate

reduces Ag^+ and produces a large number of silver nanoparticles, helping the development of silver nuclei, typical to Ostwald Ripening.

2.2.4 Ostwald Ripening

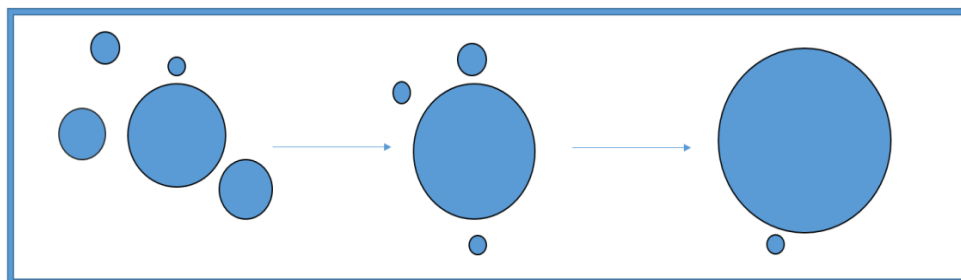


Figure 3. Ostwald Ripening: Large Particles Grow at The Expense of Smaller Particles

Optimal nanoparticle production occurs when the nucleation process is rapid and the growth process is slow. In the Ostwald ripening process (**Figure 3**), small particles dissolve and reprecipitate on the surface of larger particles in a thermodynamically-driven, spontaneous event. Minimization of surface energy is the driving force of this process.

Agglomeration and aggregation can occur at any step in the growth of nanoparticle synthesis. To stabilize the nanoparticles two strategies were demonstrated:

- i.* steric repulsion, obtained through *capping ligands*
- ii.* electrostatic repulsion.

Capping ligands are molecules that adsorb onto the surface of nanoparticles during synthesis and typically contribute to both arresting nanoparticles growth and to stabilizing the nanoparticles in solution. Given that often such ligands are long alkyl chain molecules, ligand exchange is pursued toward replacing the original capping ligands with shorter molecules.

The electrostatic interactions are attributed to intrinsic nanoparticle surface and mostly applies to salt and oxide nanoparticles, which have either cationic or anionic species present on the surface, thus driving electrostatic interactions.

Synthetic methods of nanoparticle stabilization for the nanoparticles of our interests, using the aforementioned strategies, will be illustrated in Chapter 3 (Experimental Methods).

2.2.5 Chemical Reduction in Synthesis of Metallic Nanoparticles

The chemical reduction of a metal cation is necessary for the precipitating metals from aqueous or non-aqueous solutions [14]. Typically, a reduction reaction of a transition metal (M) cation follows reaction (4) below,



simultaneously occurring with an oxidation process of the species X; reaction (5).



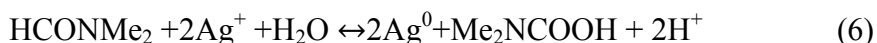
Thermodynamically, a solvated electron (e_s) in solution is the strongest reducing agent next, it is typically provided by an alkali-metal or alkaline-Earth element such as sodium or potassium [14]. Electron transfer occurs when the free energy, ΔG , and the electrode potential E° of the species to be reduced is favorable. Reducing any metal with an E° more positive than -0.481 V or -0.23 V should be plausible at room temperature given reducing reagent availability and controlled pH. Many first, second, and third-row transition elements such as Fe^{2+} , Fe^{3+} , Ni^{2+} and Cu^{2+} are capable of precipitating as metal nanoparticles from solution. In solvothermal

precipitation, the organic capping agents such as trisodium citrate act typically to prevent agglomeration and can also function as the reducing agent [14].

A large number of synthetic methodologies for producing gold (Au) and silver (Ag) nanoparticles require strong reducing agent such as sodium borohydride (NaBH₄).

In a recent reports, an ingenious method uses borohydride to reduce aqueous Ag⁺ while the bis(11-trimethylammoniumdecanoylaminoethyl) disulfide dibromide (TADDD) present in the reaction solution is simultaneously reduced by NaBH₄ to a thiol which acts as a capping ligand and arrest nanoparticles growth to 3.3 nm nanoparticles. [19]. The drawback of this method is that is requiring extra synthesis of TADDD.

In another report, precipitation of silver nanoparticles that range from 6 to 20 nm is done by reduction of non-aqueous, AgNO₃ or AgClO₄ by N,N-dimethylformamide (DMF) involves DMF oxidation to a carboxylic acid. The addition of aqueous solutions of AgNO₃ or AgClO₄ (typically microliter volumes) to DMF leads to the slow reduction of silver ions to silver metal, [20] illustrated in reaction (6) :



and can be controlled by altering the concentration [DMF]/[Ag] or changing the temperature [14]. However, this synthesis is difficult to scale up.

Thus, there is a need for improved synthetic methods to obtain Ag nanoparticles.

2.2.6 Microwave Precipitation

Reaction mixtures containing water undergo rapid heating with microwave processing, due to the large dipole moment of water, leading to rapid precipitation of nanoparticles. Therefore, microwave assisted-synthesis, beyond the energy savings, is typically characterized by short reaction times.

Preparing metal nanoparticles by microwave methods were originally studied by Fiévet et al. [21] and known as the *microwave-poly process*. The objective of this study led to significant breakthroughs synthesizing colloidal Pt with particle size ranging from 2 nm to 4 nm.

Yu et al. synthesized Pt by microwave assisted irradiation in a domestic 2450 MHz microwave oven using H_2PtCl_6 precursor in poly(N-vinyl-2-pyrrolidone), ethylene glycol and NaOH for 30 seconds and with controlled microwave frequency [22].

Additionally, Tsuji et al. used microwave irradiation and PVP to stabilize Ni in ethylene glycol [23]. Tu et al. utilized an open flow microwave reactor to synthesize Pt nanoparticles ~1.5 nm [24].

Microwave methods were also used for the preparation of nanoparticle chalcogenides such as CdSe, PbSe. Gedanken et al. used microwave refluxing of solutions containing Cd^{2+} , Pb^{2+} , or Cu^{2+} and Na_2SeSO_3 in an amine-based stabilizer to prepare the CdSe chalcogenide nanoparticles that range from 4 to 5 nm [25].

The examples above suggest that microwave-assisted methods have been successful in many nanoparticle syntheses and could be key to energy-saving, scalable nanomaterials synthesis.

2.2.7 Sol-Gel Chemistry

Sol-gel chemistry involves the gradual conversion of monomers present in a colloidal solution (sol) into a network (gel) in a shape of a polymer network or discrete nanoparticles [26–28].

Livage et al' showed that transition metals with lower electronegativity values (in the Pauling scale of electronegativity), such as Si (+0.32), are less stable when forming complexes during hydrolysis. In the case of high partial charge values for elements such as Ti (+0.63) and Zr (+0.74) stabilization during the transition state of hydrolysis is observed. Because of the high partial charge, hydrolysis of Ti and Zr complexes are fast and require special handling to avoid contact with water and oxygen [14].

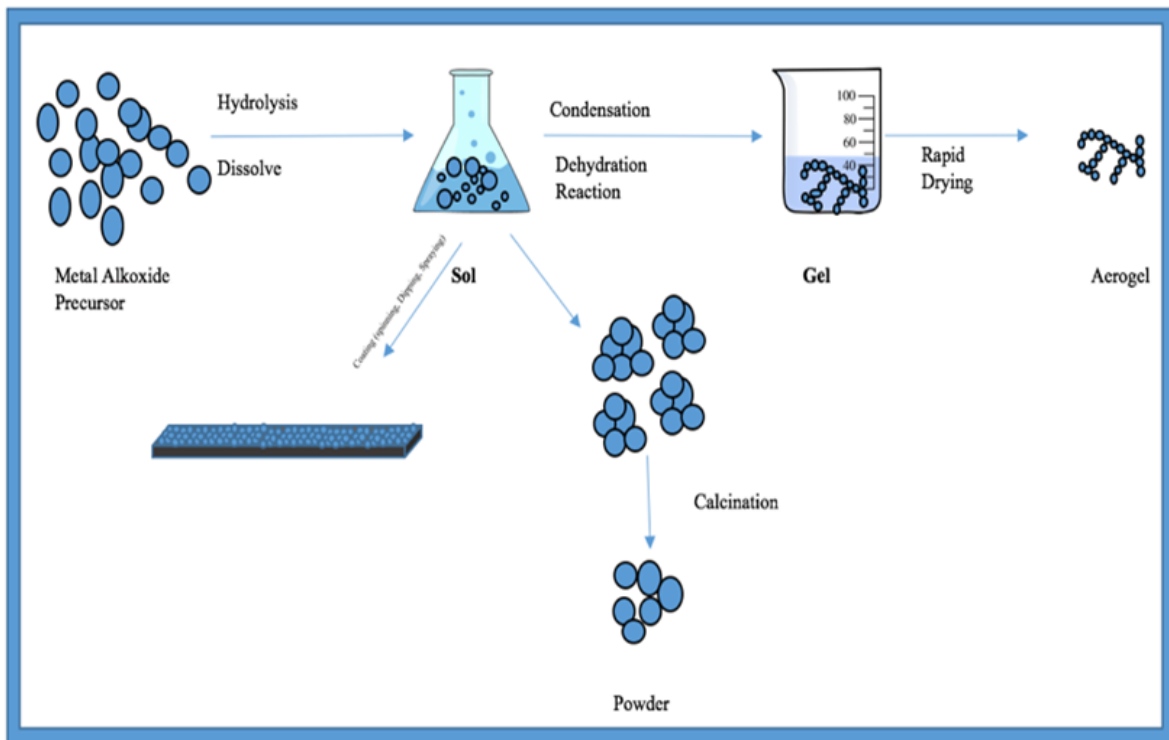


Figure 4. Sol-gel Preparation of Nanomaterials

Gel networks can be formed by acid-base catalyzed hydrolysis of metal alkoxides. Base-catalyzed hydrolysis is the preferred method for fabricating nanoparticles. Precursors structure and pH is important when tuning the size and morphology of sol-gel products [29]. Sol-gel methods are most commonly used to synthesize oxides, sulfides, nitrides, and carbides.

2.2.8 Pechini Method

The Pechini method was proposed in 1967 to produce capacitors [30]. Pechini's modification of the sol-gel method was intended for metals that don't suit traditional sol-gel reactions [31]. Pechini syntheses of metal nanoparticles [32,33] using oxalic acid, and polymeric alcohols such as PVA as chelating agents results in nanoparticles with little control of the particle size, shape, and morphology.

2.2.9 Microemulsion

Microemulsion is a versatile method for the preparation of inorganic nanoparticles. The thermodynamically stable system is composed of two immiscible liquids such as water and oil and a surfactant. The surfactant facilitates formation of droplets consisting of water-in-oil or oil-in-water. The size of droplets can be controlled by changing the ratio of water or oil/surfactant. Some factors influencing surfactant selection include considering other components of the microemulsion, especially for systems containing oxidizing and reducing agents. The surfactant Aerosol OT (sodium bis(2-ethylhexyl) sulfosuccinate, AOT) was recently introduced for its stability against mild oxidizers.

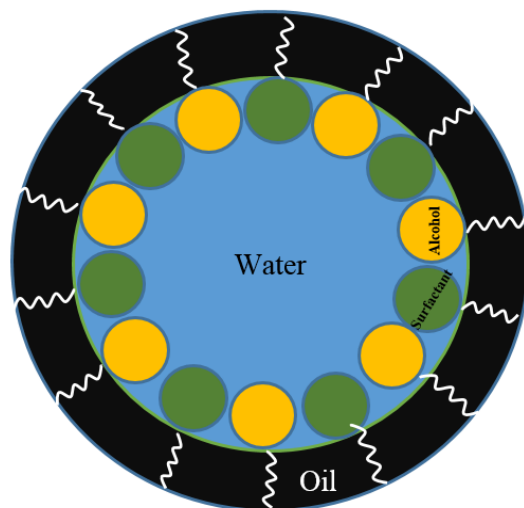


Figure 5. Diagram of Schulman's Microemulsion Model

aqueous solutions, which involves the chemical reduction of a metal cation. Chen et al. reported synthesis of Ni nanoparticles with a narrow size distribution from water-CTAB –n-hexanol [34], demonstrating that metal nanoparticles could be obtained through this method.

2.2.10 Hydrothermal / Solvothermal Nanoparticles Synthesis

Solvothermal processing involves chemical reactions conducted at high temperatures. Hydrothermal processing refers to the subset of reactions using water as solvent.

In 1988 Oguri et al. [35] reported the preparation of monodispersed TiO₂ anatase nanoparticles from Ti(OEt)₄ in ethanol.

The hydrothermal synthesis of nanocrystalline TiO₂ was also investigated by Cheng et al., for preparing nanoparticulate TiO₂ with either rutile or anatase crystal structure from aqueous TiCl₄. The report showed that strict pH control impacts the outcome; acidic conditions lead to rutile and basic conditions favored anatase [36].

New developments include microwave-assisted solvothermal process and “continuous flow” hydrothermal process for large-scale nanomaterials production.

Microwave-assisted hydrothermal processing has been used since 1992 for synthesizing oxides [37] and zeolites. One of the common uses of microwave hydrothermal method is in the fabrication of nanostructured mesoporous materials.

2.2.11 Biomimetic Synthesis

Biomimetic syntheses take advantage of nature examples in forming nanostructures, using polymeric biomaterials as templating sources. Protein folding creates nanopockets which could be used as scaffolds for nanomaterials synthesis.

Meldrum et al. demonstrated synthesis of iron sulfide (FeS_2), manganese (Mn) and uranium oxohydroxyde nanoparticles inside the ferritin iron-storage protein cages demonstrated the concept and prompted further research in the field [38]. The protein structure effectively acts as a nanoreactor to limit particle growth. Innovative research in biomimetic synthesis continues to grow and now includes protein engineering of viral cages to serve as scaffold for nanoparticles formation [39]. However, this method is not scalable for nanoparticles production and not intended for scalability. Therefore, it is not suitable for mass production of nanoparticles. However, the possibility to have templated synthesis prompted the templated synthesis approach which considering a smaller template significance and renders scalability.

2.3 Nanofluid

2.3.1 Nanofluid Materials

The term nanofluid is used to describe nanoparticles dispersed in a fluid to enhance their usability by exploring their collective [40–42] Brownian agitation of nanofluids prevents settling due to gravity. Preserving the nanoscale size is tedious because as nanoparticles come into contact with one another they tend to agglomerate and form larger particles. Provided that agglomeration does not occur in nanofluids, they are emerging in the nanomaterials field as unique materials, and recently, the number of applications have increased [43,44]. In particular, the need for highly conductive fluids [45–86] and connective fluids with heat transfer properties has geared the increase to develop nanofluids. Areas of nanofluid research include synthesis techniques, [44,87–90] and their applications [91–101]

Theoretically, simply mixing a nanopowder in a solvent could produce a nanofluid, as long as the final dispersion meets the expectations of high concentration and dispersion stability over time.

However, a nanofluid cannot always be fabricated from pure nanoparticles. Therefore, direct synthesis of nanofluids is required. The most common synthesis of nanoparticles involves solution chemistry. The chemical reduction of a metal salts in the presence a stabilizing agent is the most common method used to precipitate nanoparticles, as it was showed is section 2.2. To produce a nanofluid, such reaction further needs to operate at high concentration of precursors and to not require purification of final product.

The transport properties of nanofluids such as thermal conductivities, k , convective heat transfers, h , specific heat c_p , and viscosity, μ were first investigated Choi's group, leading to an increased interests in thermal science research [102]. In 2006 research by Buongiorno recognized the significance of convective heat transfer (h) and nanoparticle size distribution in nanofluids, suggesting that nanofluids are ideal to enhance convective heat transfer [94]. Synthetic approaches that are both sustainable and commercially feasible are therefore desired toward fostering development of nanofluids in commercial applications.

2.4 Materials Characterization

In recent years, microscopy has become a standard analytical technique used for materials characterization to obtain chemical and structural information of nanoparticles. In this work, low voltage electron microscope (LVEM5), transmission electron microscope (TEM), and scanning electron microscope (SEM) was used to study nanoparticle size and size distribution.

2.4.1 Transmission Electron Microscopy

The development of the electron microscopy (EM) enabled determination of structure and morphology of nanoscale objects.

The introduction of aberration corrections on commercially available transmission electron microscopes (TEM), the development of faster computers with access to instant aberration corrections and autotuning, made possible EM with atomic resolution (0.5 Å) to be attained [103,104].

Remarkable progression identifying possible active centers of single atoms, dimers, or trimers of metallic atoms have been achieved [105–110]. The defined Fresnel fringes on the boundary of specimens give an insight of the surface structure of nanoparticles [111–113].

Nanomaterials field has seen a tremendous growth facilitated by TEM [114,115], [112,116–126]. Details on nanomaterials characterization by TEM are presented as follows.

2.4.2 Electron Microscopy for Analysis of Nanoparticles

Besides full geometric and morphological information of a single nanoparticle, nowadays state-of-the-art TEMs capture tomographic, holographic and spectroscopic information at atomic scale. In addition, electron dispersive X-Ray diffraction embedded into TEM provides structural and compositional information at single nanoparticle level.

2.4.3 Morphological Information Acquired With TEM

TEM images enable visualization of size, shape distribution and particle size distribution of nanoparticles [127–133]. It was recently demonstrated that three-dimensional (3D) high-resolution images [134,135] of nanoparticles could be obtained with contrast techniques [136,137].

Structural Information from high-resolution TEM (HR-TEM) is performed in phase contrast and captures the atomic-structure of samples. The aberration corrector on the HR-TEM can be used to pinpoint sites on the surface of a nanomaterial [107,108,112,138]. The TEM equipped with aberration corrector and using density functional theory (DFT) models are efficient allow

capturing of atomic level images of adsorbed molecules, thus enabling imaging of ligands on particle surface and potential structural changes occurring upon ligand exchange.

2.4.4 Developments of TEM

The development of X-ray detectors has simplified and improved the composition, analysis and element mapping in 3D. Integrating detectors close to a sample has improved the X-ray collection accuracy [139] reducing the time for 3D mapping from hours to minutes.

Efforts for capturing 3D images from two-dimensional (2D) TEM projections began in the 1960's [140,141] and was mainly used to research structural biology. The introduction of the charged coupled device (CCD) camera, automation of microscopy and development in computational techniques aided the advancements of electron tomography [117]. The driving force of electron tomography in 3D imaging of mesoporous materials and space distribution has been published in many reviews.

Advanced research of ultrafast or fourth dimension (4D) EM has been developed by Zewail et al. The fourth domain refers to the time scale and it provides data on real, reciprocal and energy space by EM allowing research of fast chemical phenomena such as bond forming or breaking.

2.4.5 Low Voltage Electron Microscopy

Generally, TEM's operate between 200-300 kV. The higher the energy of electrons the more likely they can cause the knock-on effect [142] on materials such as carbon where knock-on

collisions of the electrons are knocked on to materials causing displacement, modification and bond breaking of the material.

High-energy electrons carry high momentum causing high-angle elastic scattering by atomic nuclei which could transfer several eV or tens of eV to each nucleus, giving rise to knock-on displacement damage. For crystalline nanoparticles, this is represented by displacement of atoms from lattice sites, producing interstitial atoms and vacancies; thus, resulting TEM images not only damage but importantly, misrepresent the actual sample [143].

To avoid the knock-on for carbon the threshold is around 80 kV [144] and operating below this threshold is preferred. Recently, low-voltage TEM (20-80 kV) [145,146] is selected to minimize sample damage, especially when working with biological samples. Further innovations in low-voltage EM revolutionized imaging of biological samples. In the research described in the thesis, we have extensively used a low voltage electron microscope, which is described in detail in the following section.

2.4.6 Low Voltage Electron Microscope 5 kV (LVEM5)

The LVEM5 enables capturing images of nanoscaled particles at a small accelerating voltage of 5 kV and a resolution of 2.5 nm.

Presently, EM take up a lot of space and require a highly skilled technician to capture images. Additionally, a conventional EM operates at an accelerating voltage 200-400 kV. DeLong Instruments has established an innovative low voltage EM that operates at a

substantially low voltage, ~5 kV, improving contrast and successfully image nanomaterials in five different modes.

The design of the LVEM5 is like no other traditional electron microscope and is ~1/10 of its size. The LVEM5 is equipped with a small Schottky field-emission gun (FEG), magnet condenser, and objective lenses, a YAG screen for capturing images using light optics, a CCD camera for imaging, a small vacuum chamber and delivers fast sample exchange for high-throughput screening. The pumping unit comprises of two miniature ion pumps connected to the optical chamber and sits on the floor doesn't require cooling water for operating the microscope, therefore the instrument does not require special housing. The morphology of nanoparticles can be easily captured making the LVEM5 a powerful tool for looking at nanoscale particles, inorganic nanoparticles, and crystalline samples [147].

2.4.7 Nanomaterials Visualization

Innovative achievements in materials science are the identification of metal complexes, recognizing individual atoms, or oligomers on supported catalyst for presumed active sites to determine their role in catalysis [107,110,148–150]. The atomic structure of individual metal nanoparticles can be explored and resolved [134,151–153] with EM. The user-friendly TEM and CCD techniques provide a wealth of valuable imaging methods for capturing the structure of small particles (<15 nm in size) [135,154].

Multiply twinned or single crystalline is the most reported particle structures. Metal particles with these structures were first reported by Ino [153] to explain the radical (111) spots seen in

gold electron diffraction patterns and image contrast. The HR-TEM identified the multiply twinned particles (MTP) of gold and have since been studied. The most common MTP structure studied since 1980 are dodecahedron and icosahedron as well as cuboctahedron. Further image simulations are used for accurate explanations of the lattice fringes [155,156]. The study of platinum nanoparticles growth imaged with TEM at less than 10 mbar air at 650 C° increased in diameter was demonstrated in-situ [157].

2.4.8 Sample Preparation

To capture an image two factors must be considered. First, the TEM sample should be very clean and without contamination. Plasma cleaning or prior thermal treatment to eliminate any contamination is especially important as absorbed hydrocarbon or water can accelerate the electron beam and impair the image collection. The sample holder is also subjected to cleaning with mild solvents such as ethanol or methanol.

2.4.9 Side-Effects of TEM Grids

Typically, the sample to be analyzed is well dispersed in methanol or ethanol and a drop (50 microliters) of the dispersion is dispensed onto a special TEM sample holder consisting of a metal grid (usually made of copper) coated with an ultrathin carbon film. Other grid materials included are often made of Ni, Mo, or Au. The grids and samples are under electron beam irradiation, at high temperatures, or in a reactive gas, therefore their stability is critical to accurate sample imaging. Zhang et al. studied the stability of Ni, Cu, Au, and Mo grids coated

with very thin alpha-carbon. Upon dispensing the samples, the grids containing the samples were heated up to 500 °C -800 °C in a TEM. Each grid generated nanoparticles on the supported film. The study concluded that Ni grids could not be used in conjunction with carbon because the Ni nanoparticles produced graphitization of amorphous carbon. However, Mo and Au grid exhibited good stability at very high temperatures of 680 °C -850 °C under a TEM vacuum [158].

The possibility for TEM grids or grid-coating films to generating artifacts complicates *in situ* studies at high temperatures. For instance, Zhang et al. showed that while studying Pt nanoparticles in carbon nanotubes supported on a Cu grid, the Cu atoms diffused into the Pt-filled CNT at 600 °C to create a Pt-Cu alloy [158]. Therefore, a careful selection of TEM grids is needed prior TEM image analysis.

2.4.10 Conclusion

The progress of the EM facilitated the advancement of nanoscale materials. Nowadays, the EM is viewed as a nanolaboratory with the ability to characterize morphological, crystallographic, compositional and electronic properties of materials.

TEM nanolaboratory for experimenting and monitoring the dynamics of the nanoparticles is one of the most difficult aspects of TEM applications in materials science. However, there are still developments in hardware and applications methods that need to be addressed.

From a general viewpoint, the relationship between cost and value of EM in practical analysis of structural complexity cannot be underestimated. In fact, the application potential of the TEM is underused because of a shortage of expert knowledge of analysis and operating the

TEM. In the case of low-voltage microscope such as LVEM5, the use of a small-sized instrument which does not require a dedicated operator and special housing, enables high-throughput analysis and thus speeds up nanoparticles research.

CHAPTER 3. EXPERIMENTAL

3.1 Materials

Zinc acetate dihydrate ($\text{Zn}(\text{O}_2\text{CCH}_3)\cdot 2 \text{H}_2\text{O}$) was purchased from Alfa Aesar Ward Hill, Massachusetts, U.S.A. Poly(vinyl alcohol) (PVA) ($\text{C}_2\text{H}_4\text{O}_n$), was purchased from Polysciences, Inc. Warrington, Pennsylvania, U.S.A. Sodium hydroxide (NaOH) pellets were purchased from Mallinckrodt, Inc., KT. Nanopure water (18.2 M Ω cm) from an ELGA Purelab Flex system was used in all solutions. High precision microwave reaction (10-20 mL type, Biotage) glass vials. (TEM) grids were purchased from Pacific Grids-Tech (<http://www.grid-tech.com>).

Silver nitrate (AgNO_3), iron (II) sulfate heptahydrate ($\text{FeSO}_4 \cdot 7\text{H}_2\text{O}$), and sodium citrate dehydrate ($\text{C}_6\text{H}_5\text{Na}_3\text{O}_7 \cdot 2\text{H}_2\text{O}$), were purchased from Sigma-Aldrich Co. Surfynol 465 and Surfynol 61 which was obtained as a donation from Air Products (www.airproducts.com).

Glass Neuvitro Assistant cover slips (24 mm x 24 mm) were purchased from NeuVitro (<http://www.neuvitro.com>). Conductivity was measured using a two-probe CEN TECH digital millimeter.

Commercially available silver nanoparticles with dimensions of 5, 10, 20, 30, 50, 70, 80, 100, and 200 nm were purchased from NanoComposix (<https://nanocomposix.com>). A silver colloidal solution with particle size of 0.65 nm was purchased from Purest Colloids (<https://www.purestcolloids.com>). The silver products were stored away from light and refrigerated at 2-8 °C. All reagents were of analytical grade and were used as received without further purification.

3.2 Instrumentation

A short description of each technique is presented as follows these techniques can pertain to typical nanomaterials including nanoparticles, nanowires, and nanoplates.

TEM

We evaluated the nanoparticles by TEM and LVEM5 toward determining particle size and particle size distribution.

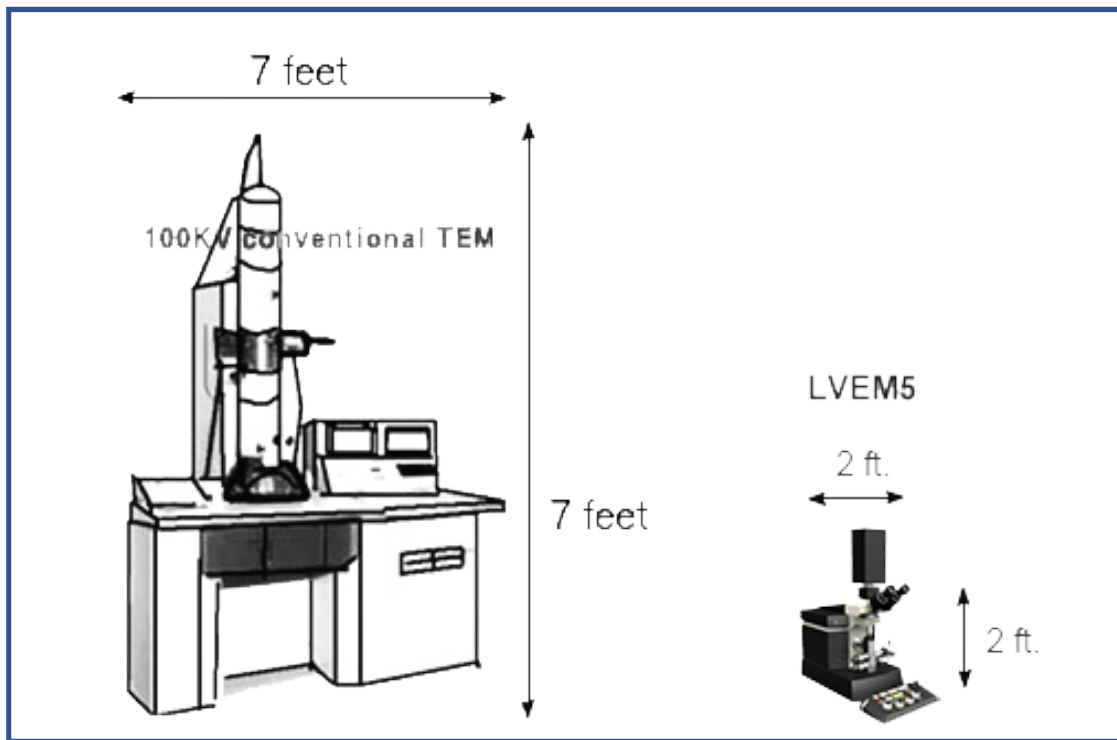


Figure 6. Size Comparison of Typical TEM and LVEM5 TEM

The LVEM5 and TEM have their own advantages and disadvantages, as described in Chapter 3. **Figure 6** shows a side by side diagram of an LVEM5 and a conventional TEM. The LVEM5 records images on low voltage, and it is a fourth of the size of a conventional TEM. The LVEM5 records images on low voltage, and it is a fourth of the size of a conventional TEM.

Sample preparation for the LVEM5 does not require staining prior to imaging. The LVEM5 used in this research is equipped with a Qcompute software package that measures particle size, enabling fast nanoparticle size characterization.

XRD

XRD of nanomaterials were obtained on a Rigaku MiniFlex 600. XRD measurements are completed to verify the materials crystalline phase and orientation between atoms. XRD is a primary method for determination of the of nanocrystals diameter (D) from the full width half-maximum (FWHM) of the main XRD peak, by using the Scherrer equation (Equation 7) [159]. The coefficient K is a constant 0.9, and the X-Rays wavelength (λ) is 1.54 Å (or 0.154 nm), the integral breadth (β) is the width of a rectangle with the same height and area as the diffraction peak or the FWHM of the peak. Theta (θ) is half of Bragg angle in rad. Standards for XRD materials analyses are available in the Joint Committee on Powder Diffraction Standards (JCPDS) database.

$$D = \frac{K\lambda}{\beta \cos(\theta)} [nm] \quad (7)$$

FT-IR

FT-IR measurements are performed on a Nicolet 6700 (Thermo Fisher Scientific) with the Attenuated Total Reflectance (ATR) accessory. For this analysis, the sample was prepared at room temperature without any dilution in KBr. The disadvantage of this is that it requires a

larger sample amount. FT-IR data evaluates absorption, and transmittance at IR wavelengths. FT-IR data is often used to identify chemical compounds and substituent groups at IR wavelength. A broadband collimated IR source is used to generate a wide range of frequencies which are passed through the sample. When the frequency of the IR radiation is the same as the vibrational frequency of a chemical bond, absorption occurs. Homonuclear diatomic molecules have a zero dipole moment across their bonds and are IR inactive.

UV-Vis

Absorbance of nanoparticles in solution was measured on a UV-Vis spectrophotometer (Scientific Evolution 201 Thermo-Scientific).

UV-Vis is a high throughput screening method. The UV-Vis spectrophotometer single beam and monochromators convert the lamp light into a discrete wavelength. The light is then passed through a sample and the output is detected by a photodiode.

The data collection method is based on the determination of transmittance as the relation between the ratio of the transmitted power $P(\lambda)$ over the incoming power $P_0(\lambda)$ for light wavelength λ . The device provides the absorbance defined as the following:

$$A(\lambda) = -\log\left(\frac{P(\lambda)}{P_0(\lambda)}\right) \quad (8)$$

PTL

PTL experiment is an alternative way to study absorption. The method is based on the detection of the amount of heat released in the sample following the absorption of light photons.

In pump-probe PTL experiment, the light from a pump laser is focused on the sample generating a thermal lens (TL). The TL is then tested by a collimated probe beam of light which propagates collinearly to the pump beam. The presence of the TL distorts the wavefront of the probe beam inducing changes in its diffraction pattern at the far field. The relative transmission of the probe light is measured through a small aperture located at the far field. Thus, the PTL signal can be defined as:

$$s(z, t) = \frac{T(z,t) - T_0}{T_0} \quad (9)$$

Where T_0 is the probe light transmission through the aperture in the absence of the pump field and $T(z, t)$ is the probe light transmission in the presence of the pump field. The signal has been written as a function of time t and sample position z . A model based on the Fresnel diffraction approximation shows that the PTL signal is proportional the fraction of the absorption used for generation of heat. Therefore, we can write:

$$S_0(\lambda) = KP(\lambda)\psi(\lambda)A(\lambda) \quad (10)$$

Where $\Psi(\lambda)$ is the quantum yield of thermal absorption and K is a constant which does not depends on the wavelength. Thus, for a sample exhibiting only absorption and scattering, the absorption and scattering cross-sections can be written as:

$$\sigma_{abs}(\lambda) = \psi\sigma(\lambda) \quad (11)$$

$$\sigma_{sca}(\lambda) = (1 - \psi) \cdot \sigma(\lambda) - \sigma_{abs}(\lambda) \quad (12)$$

Because the PTL signal does not include the scattering contribution we expect that its dependence on the diameter should be of third order with no 6th order component for any wavelength. Below we provide experimental confirmation of this fact.

PTL spectrometry uses a pump- probe lens, broadband arc lamp, and filters. Monochromatic radiation between 370 and 730 nm is the pump light source and is focused on the sample to generate a photothermal lens and measure absorption, scattering, and fluorescence contributions of the sample. The use of a He-Ne laser produces a signal proportional to the absorption of light. The amplitude obtained contains information about the magnitude of the absorption to understand the interaction between light and nanoparticles. The absorption of heat in the sample due to the light generates a thermal lens. The two-beam design provides spectroscopic and time dependence data of the sample. In a continuous wave (CW) of PTL mode-mismatched scheme, the probe beam has larger dimensions than that of the pump beam and produces a signal-to-noise ratio larger than mode-matched scheme. In a mode-mismatched the probe beam is collimated and the pump is focused generating high sensitivity of absorption in liquids [160,161].

To perform PTL experiments we used a mode-mismatched experimental scheme where the pump beam is focused and the probe beam is collimated [162]. Z-scan PTL is experiments is conducted at the same pump wavelengths (*405, 532 and 671 nm*) used for the analysis of the absorbance experiment. The experimental set-up is shown in **Figure 7**. Diode lasers generating at *405, 532 and 671 nm* provide the pump beam. The pump light is focused onto the sample (S) using a mirror (M₁) and a *15-cm* focal length lens (L₁) to generate the TL on it. A beamsplitter (B₁) redirect a small amount of the pump light toward a reference detector (Ref). The reference detector is connected to a digital oscilloscope (OSC) for triggering purposes. A signal generator

provides the modulation of the pump beam. The pump light is modulated at low frequencies ($0.1\text{-}2\text{ Hz}$) to make sure the signal reaches its stationary value. Behind the sample, the pump beam is depleted using an interference filter (F). A 2 mW He-Ne laser (632 nm) generates the probe beam. A telescope (Col) is used to collimate the probe beam up to a diameter of 3 mm . Considering the beams Gaussians we estimated the Rayleigh ranges for the pump and the probe beam as $z_e=0.7\text{ cm}$ and $z_p=100\text{ cm}$, respectively. The probe beam is directed collinearly to the pump beam using a beam splitter (B_2). The TL distorts the wavefront of the probe beam. Behind the sample, the probe beam is redirected toward a small aperture (A) and then to a diode detector (Sig) which measures the transmission of the probe light through the aperture. The generated electronic signal is amplified using a current preamplifier (Stanford Research SR 570) and then is redirected to a digital oscilloscope (Tektronix TDS3052) for processing. For the PTL experiments, we used glass cells of 0.1 cm pathlength.

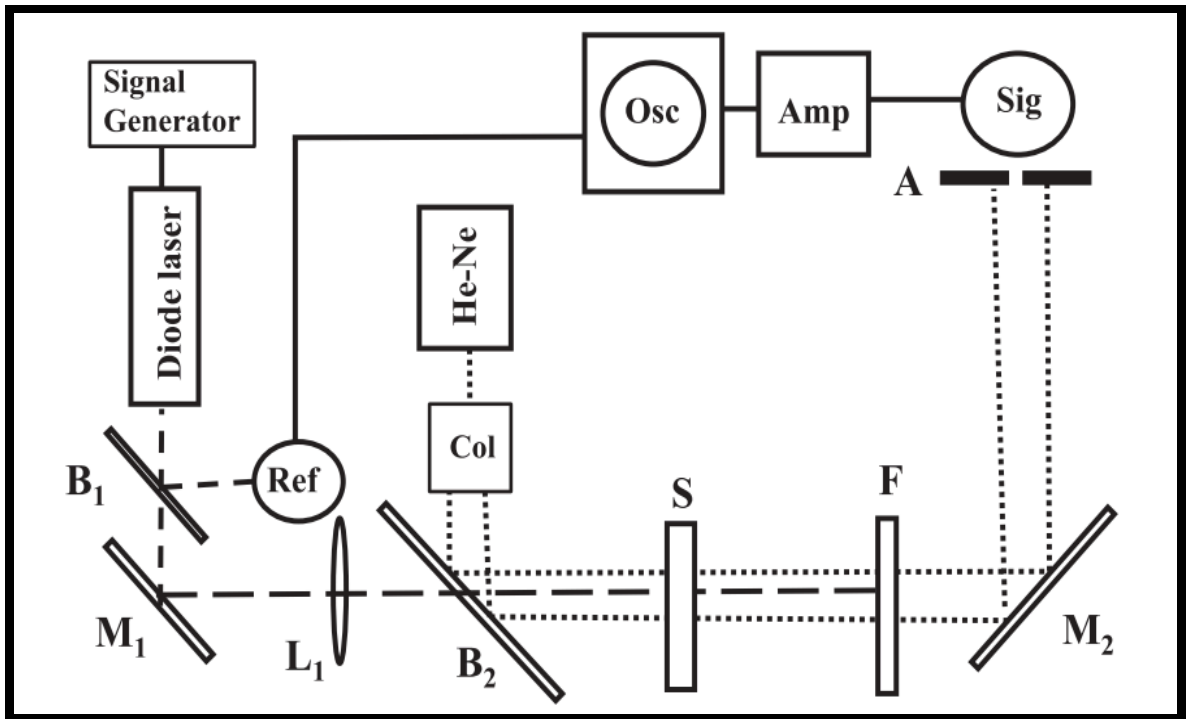


Figure 7. Schematic Diagram for PTL Experiment

Plasma Cleaner

A cleaning process is critical for producing non-contaminated surfaces. Each glass Neuvitro Assistant coverslip was treated by a plasma cleaner (PDC-001-HP, Harrick, Plasma). To avoid contamination on the substrate surface and assure that the substrate was thoroughly cleaned the coverslips were excessively cleaned before. To increase adhesion, reduce defective locations, and resistivity the substrates were annealed after by plasma.

Microwave reactors

The microwave reactions were performed in a sealed microwave vial equipped with a magnet stir bar and heated in a Biotage initiator microwave reactor (**Figure 8**). There are many advantages of microwave reactions over conventional heating. The benefits of microwave heating include the acceleration of reactions, higher yields, improved purity. Unlike conventional heating, microwaves are rapid energy transfer. Once the Microwaves are turned on, they can deliver up to 300 W of power to the sample quickly. Whereas with conventional heating it takes time for the energy to be applied.

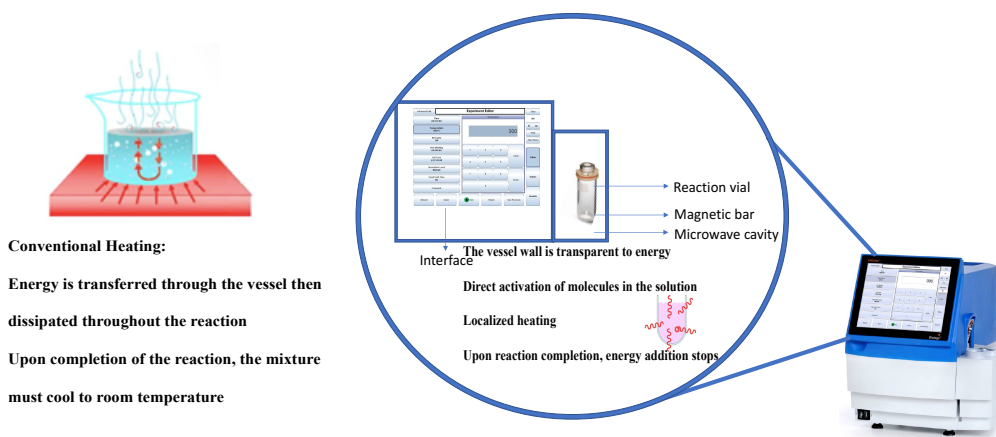


Figure 8. Conventional VS Microwave Heating

Spin Coating

Silver nanofluid samples were deposited on glass substrates by the spin coating method to prepare silver thin films at room temperature. Spin coating method is a quick and easy technique for fabricating uniform nanoparticle films from stable dispersions. This process allows adjustable thickness by disk rotation and controlled outcome of the final product.

Spray Coating

An effective alternative method for coating films is by spray deposition. A commercially available airbrush was used to spray-coat solutions of metal on glass substrates. The high level of repeatability makes spray-coating a promising method for fabricating thin film materials.

3.3 Characterization Methods

Zinc Oxide (ZnO) Nanoparticle Characterization Methods

Powder X-Ray diffraction (XRD) measurements were performed on a Rigaku MiniFlex 600 to determine crystal structure of zinc oxide nanoparticles. A sample of ZnO nanoparticles was ground to a fine powder using an agate mortar and pestle to break all aggregates. Subsequently, the powder was packed in a glass sample holder and evaluated at a voltage of 30 kV and a current of 10 mA with a Cu K_{α} source of X-rays ($\lambda=1.54051 \text{ \AA}$). A MiniFlex grid software package from Rigaku was used to process the powder XRD data.

Fourier transform infrared (FT-IR) spectrometry measurements were performed on a Nicolet 6700 (Thermo Fisher Scientific). FT-IR was used to identify chemical composition of the capping ligands on the surface of zinc oxide nanoparticles. Ground samples were compressed into a thin film disk. Transmission mode was used with an Attenuated Total Reference (ATR) sampling accessory and a zinc selenide crystal.

For a high-throughput screening of zinc oxide nanoparticles the low voltage electron microscope (LVEM5) was used in transmission mode. Sample preparation methodology for the LVEM5 is critical to capturing the highest quality images. ZnO nanoparticles were collected by centrifugation and redispersed in nanopure water via sonication. The sonication was routinely performed with QSonica Sonicator probe in the pulse mode, at 19% amplitude for 2 minutes to prevent heat build-up.

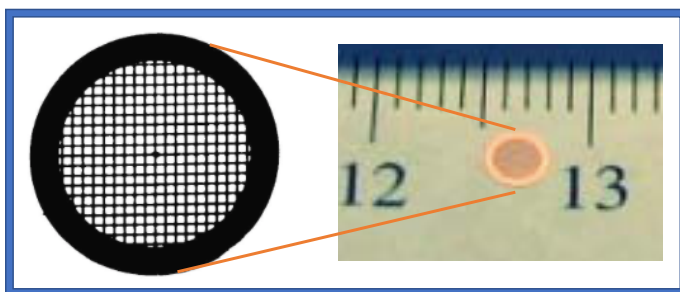


Figure 9. TEM Grid

To examine the ZnO nanoparticle on the LVEM5, $\sim 0.2 \mu\text{l}$ of the prepared ZnO nanoparticle solution sample was deposited onto a holey carbon support film on Cu in 300 mesh high definition TEM grids (**Figure 9**). To validate high-throughput measurements; additionally,

a Zeiss LIBRA transmission electron microscope (TEM) was used and images were captured at a high voltage.

Optoelectronic properties were studied using an ultraviolet-visible (UV-Vis) spectrophotometer on a Scientific Evolution 201 Thermo-Scientific. UV-Vis spectra of ZnO solution samples were collected by adding 1 mg of ZnO with 1 ml of nanopure water followed by 15 min of sonication in a water bath. Absorption spectra in the ultraviolet and visible regions were obtained in the range of 190-1100 nm. The cells were rectangular quartz cuvettes with 1 cm path length. Nanopure water was used as a blank. For each sample the spectrum was collected at room temperature.

In-House Synthesized Silver (Ag) Characterization Methods

The size and morphology of the nanoparticles were analyzed by Zeiss LIBRA TEM. The sample was prepared by placing 2 μ L of silver nanoparticles suspension on a carbon-coated copper grid and subsequently air drying it, before transferring it to the microscope operated at an accelerated voltage of 120 kV.

The optical properties of silver nanoparticles were examined by UV-Vis spectroscopy. Silver nanoparticles were dispersed in nanopure water at a stock solution concentration of 32.75 mg/mL. Various dilutions were prepared from the stock solution by serial dilution. 0.5 mL of the stock solution suspension was mixed with 1 mL nanopure water. 0.5 mL of this suspension was labeled C₁ and when mixed with 1 mL nanopure water served as C₂ dilutions and so on until 4 dilutions were achieved (C₁-C₄). Absorption spectra were obtained using a UV-Vis spectrophotometer (Scientific Evolution 201), in the range of 190-1400 nm using a rectangular

quartz cuvettes with 1 mm path length. PTL signal experiments used glass cells of 0.1 cm path length. For each concentration, a blank with nanopure water was used to correct any sample absorbance.

Commercially Available Silver (Ag) Nanoparticle Characterization Methods

A UV-Vis spectrophotometer was used to validate the NanoComposix absorbance spectra of each of the solution samples. Aqueous solutions of samples at the concentration of 0.02 mg/mL were measured in standard 1-cm path length quartz cell cuvettes.

Photothermal Lens (PTL) spectrometry measurements used glass cells of 0.1 cm path length. Nanopure water was used as a reference. Samples for UV-Vis and PTL were measured for three different wavelengths: 405, 523 and 671 nm.

3.4 Synthesis of Zinc Oxide

In a typical experiment, a 0.0042 M (1.05 g, 0.042 mmol) solution of polyvinyl alcohol (PVA) was prepared in nanopure water. A 0.68 M (0.75 g, 3.4 mmol) solution of zinc acetate dihydrate ($\text{Zn}(\text{CH}_3\text{COO})_2 \cdot 2\text{H}_2\text{O}$) was prepared in nanopure water. Meanwhile, a 2.5 M (0.5 g, 12.5 mmol) solution of sodium hydroxide (NaOH) was prepared in nanopure water. All three solutions were heated at 92 °C and stirred at 500 rotations per minute (RPM) for 20 minutes to ensure complete homogenization [163].

Next, the PVA solution was added into a 20 mL microwave reaction vial. Subsequently, the $\text{Zn}(\text{CH}_3\text{COO})_2 \cdot 2\text{H}_2\text{O}$ solution was added to the PVA solution followed by the NaOH solution, leading the final solution to turn opaque (white cloudy) (**Figure 10**). Then the vial was immediately placed in the microwave reactor and the reaction parameters were set through the interface software to various times, per experiment design; with prestirring (1 minute); reaction stirring and temperature 90 °C. A white precipitate formed upon the microwave reaction. The reaction mixture was centrifuged (15 minutes, 7400 RPM) to separate the nanoparticles. The obtained pellet was further purified by adding ethanol and redispersing the particles for removing excess PVA. The particles were further collected by centrifugation (15 minutes, 7400 RPM) and the process was repeated with methanol and nanopure water. After the final wash, an aliquot of the nanoparticle pellet was redispersed in nanopure water for various analyses and the rest of nanoparticles were dried overnight in a vacuum [164–167].

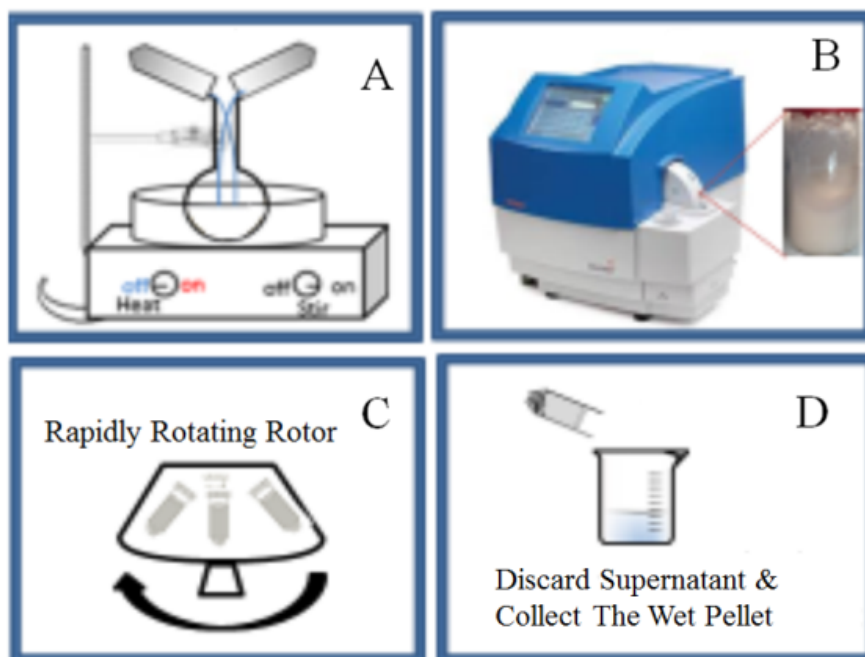


Figure 10. Schematic of Zinc Oxide Nanoparticle Microwave Assisted Synthesis

3.5 Synthesis of Silver

Silver nanoparticles were synthesized by a chemical reduction method. All reagents were dissolved in nanopure water.

In a typical experiment, an aqueous solution of trisodium citrate ($C_6H_5Na_3O_7$) 1.45 M (18 g, 69.7 mmol) was prepared in 48 mL of nanopure water and vortexed for approximately 1 min then cooled in a 10 °C ice bath. Next, a solution of 0.83 M (9 g, 32.4 mmol) iron II sulfate heptahydrate ($FeSO_4 \cdot 7H_2O$) was prepared in 39 mL of nanopure water, vortexed for ~1 min and kept at room temperature. A solution of 0.54 M (17.6 mmol) silver nitrate ($AgNO_3$) (3 g) was prepared in 48 mL of nanopure water and vortexed then cooled in a 5 °C ice bath. The precooled trisodium citrate solution was slowly poured into a 250 mL round bottom flask equipped with a stir bar and set in a crystallizer filled with ice (**Figure 11**). To this solution, the iron sulfate and precooled silver nitrate solutions were combined simultaneously and the final solution was mixed vigorously for 10 min. The color changed from white to crimson red. The change in color can be understood as the reduction of Ag^+ to Ag^0 proceeds. After the reaction, particles were collected by centrifugation for 15 minutes, at 7400 RPM (**Figure 12**). The supernatant was discarded and the pellets were further dispersed in nanopure water to form a nanofluid.

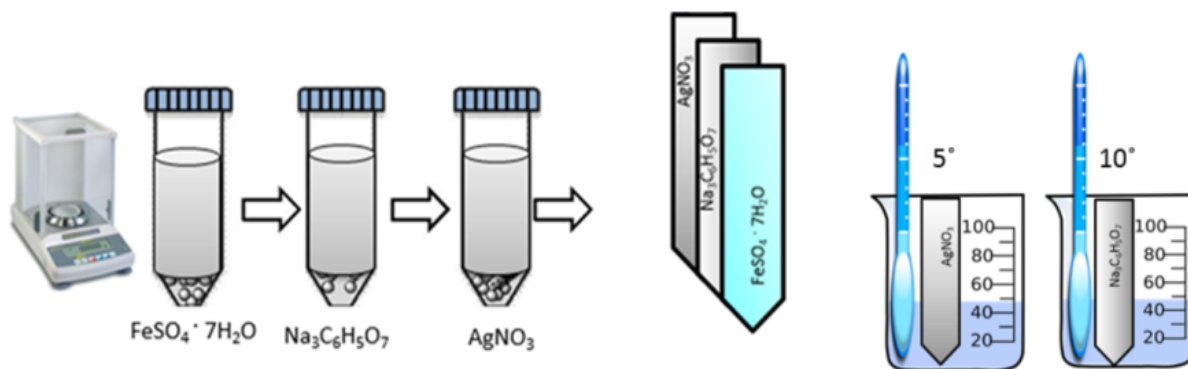
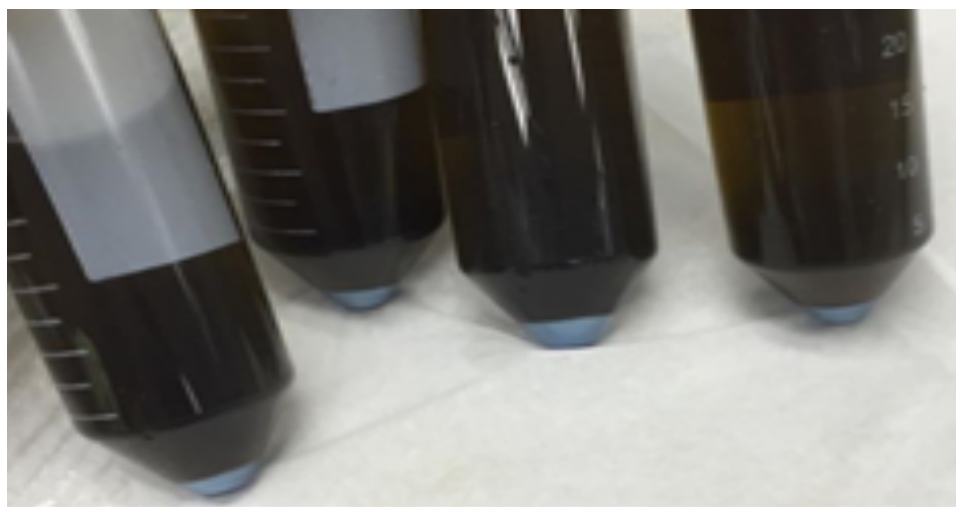


Figure 11. Schematic of In-House Synthesized Silver Nanoparticle Synthesis

Figure 12. Collected Reaction Mixture (Wet Pellet)



3.6 Fabrication of In-House Synthesized Silver Inks

Preparation of Ink 1

25 μ l of Surfynol 465 was combined with 1 mL of in-house synthesized silver nanoparticle solution and probe sonicated for 2 min. The solution was cooled and a final reddish-brown solution was obtained.

Preparation of Ink 2

25 μ l of Surfynol 61 was added to 1 mL in-house synthesized silver and probe sonicated for 2 minutes while the ink was cooled in an ice bath. A final 1 mL dark green ink solution was obtained indicating a color change as a result of the addition of Surfynol 61.

3.7 Fabrication of In-House Synthesized Silver Films

Silver films were produced via 2 methods spin coating and spray coating the inks on glass Neuvitro Assistant coverslips (24 mm x 24 mm). Both methods begun by pre-cleaning the glass surface in a sonicating bath with soapy water, followed by acetone, then rinsing the glass with nanopure water. The glass slides were further treated by a Harrick Plasma PDC-001-HP plasma cleaner filled with argon gas (5-10 psi) set to a high radio frequency (RF) power of 30 W for 1-3 min. The plasma precleaned glass surface allowed for better adhesion of the inks.

Next, thin films were prepared using spray coating and spin coating, to compare the experimental results. To prepare a one-layer coating, 80 μL of stable silver nanoparticle ink was deposited on the center by spin coating, or spray coating (**Figure 14a-c**).

The solutions were deposited by spin coating method on glass slides mounted on motor axel rotating at 750, 1500, and 3000 RPM consecutive stages. The film samples were annealed for 1 to 3 min by vacuum plasma treatment under argon to reduce resistivity and enhance the characteristics of the silver films (**Figure 14c**).

The airbrush, a commercially available Iwata Eclipse HP-CS airbrush, was powered by an oil-less compressor (piston type) at 1-35 psi to prevent droplets. The working distance of the airbrush to the glass slide was varied from 5-10 cm. Additional control of the deposition conditions was achieved by the speed and direction of the airbrush to build up the active layer of several ultra-thin layers. The stenciled spray coating in **Figure 13** was achieved by coating one layer of stable Ag ink 1.

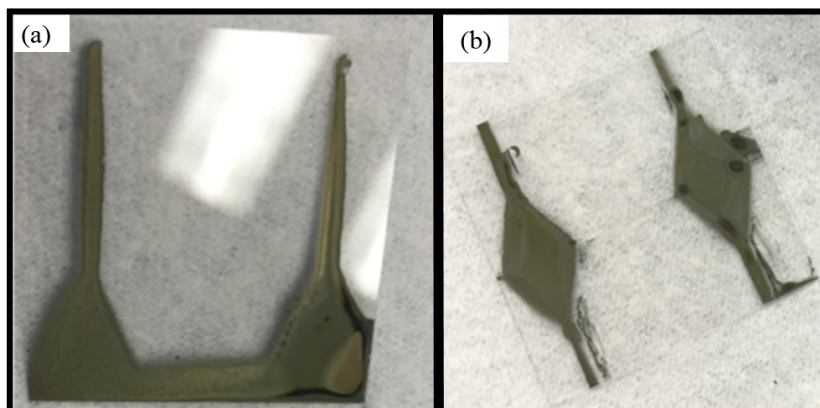


Figure 13. One Layer Spray Coating of Ag Sample Ink 1 (a) Plasma Treated (b) Without Plasma Treatment

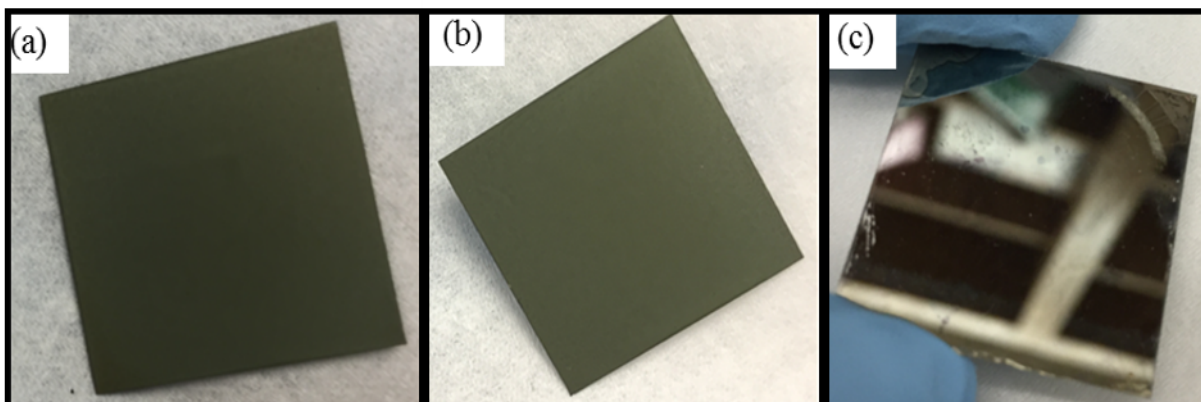


Figure 14. One Layer Spray Coating of Ag (a) & (b) Sample Ink 1 (c) Spin Coating of Sample Ink 2

CHAPTER 4. RESULTS AND DISCUSSION

4.1 Characterization of Synthesized Zinc Oxide Nanoparticle

As outlined in the Experimental section, the characterization methods used for in-house synthesized zinc oxide include XRD, FT-IR, LVEM5, TEM, and UV-Vis. The shape, size and crystallinity of the synthesized zinc oxide nanoparticles were analyzed using a combination TEM, LVEM5 and XRD. According to XRD analysis, the crystal structure of synthesized zinc oxide nanoparticles is hexagonal wurtzite with diameters ranging from 15.8 nm - 20.9 nm depending on the reaction time, which relates to particle growth (**Table 1**).

Table 1. Properties of Zinc Oxide Synthesized in Our Lab

Sample	Reaction time (min)	Synthesis	Solvent	PVA (g)	Average Crystal Size (XRD) (nm)	Average Particle size (TEM) (nm)	Percent Yield
1	5	Microwave	Nanopure water	1.05	16.76	50-75	91.5
2	20	Microwave	Nanopure water	1.05	20.97	50-75	90.6
3	25	Microwave	Nanopure water	1.05	16.6	25-50	98.5
4	30	Microwave	Nanopure water	1.05	15.8	25-50	68.2
5	60	Conventional	Nanopure water	1.05	ND	ND	48.5

ND: not determined

The morphology of synthesized zinc oxide nanoparticles were characterized by TEM and LVEM5. The zinc oxide nanoparticles present a spherical morphology. FT-IR was used to identify the chemical composition of zinc oxide powder samples and UV-Vis was used to confirm the optoelectronic properties in absorption patterns.

XRD Characterization

The XRD of zinc oxide nanoparticles was carried out on a Rigaku MiniFlex 600 using sample Cu K_{α} radiation. To identify the compound and investigate the purity of zinc oxide its phase structure and crystal size of zinc oxide nanoparticles XRD spectra of aliquots were collected at different time intervals and studied. All samples of zinc oxide nanoparticles show the appearance of wurtzite peaks with hexagonal phase. The major diffraction peaks are in agreement with the standard card JCPDS 36-1451 which 2θ at 31.68° , 34.36° , 36.18° and 56.56° are indexed as (100) (002) (101) (102) and (110) planes of hexagonal wurtzite structure. The length of time affected the percent yield.

The crystallite size was determined by using Scherrer's equation (**Equation 7**). The zinc oxide exhibited a crystal size of 16.76 nm in sample 1 according to the higher intensity and sharpness of all peaks as shown in **Figure 15a** and a crystal size of 16.6 nm after 25 minutes (**Figure 15b**). The decrease in size was supported by the decrease of peak intensity and that peaks became broader. The smaller crystal size may be characteristic to faster particle growth. The most intense peak is obtained along (101) orientation. The extreme intensity of the diffraction peak indicates that the synthesized ZnO sample is well crystallized and of high purity. Whereas line broadening of diffraction peaks in Figure 15b is attributed to particle size effects.

Interestingly, the different FWHM of the (002) diffraction line compared with the (100) and (101) peak was observed and the ratio of (100) and (002) increased in sample 1 when compared to sample 3 (**Figure 15**) indicating that the particles obtained from sample 3 are smaller than the particles obtained from sample 1 as confirmed by TEM (**Figure 16**). No characteristic peaks of any impurities were detected, suggesting that high-quality zinc oxide nanoparticles were synthesized.

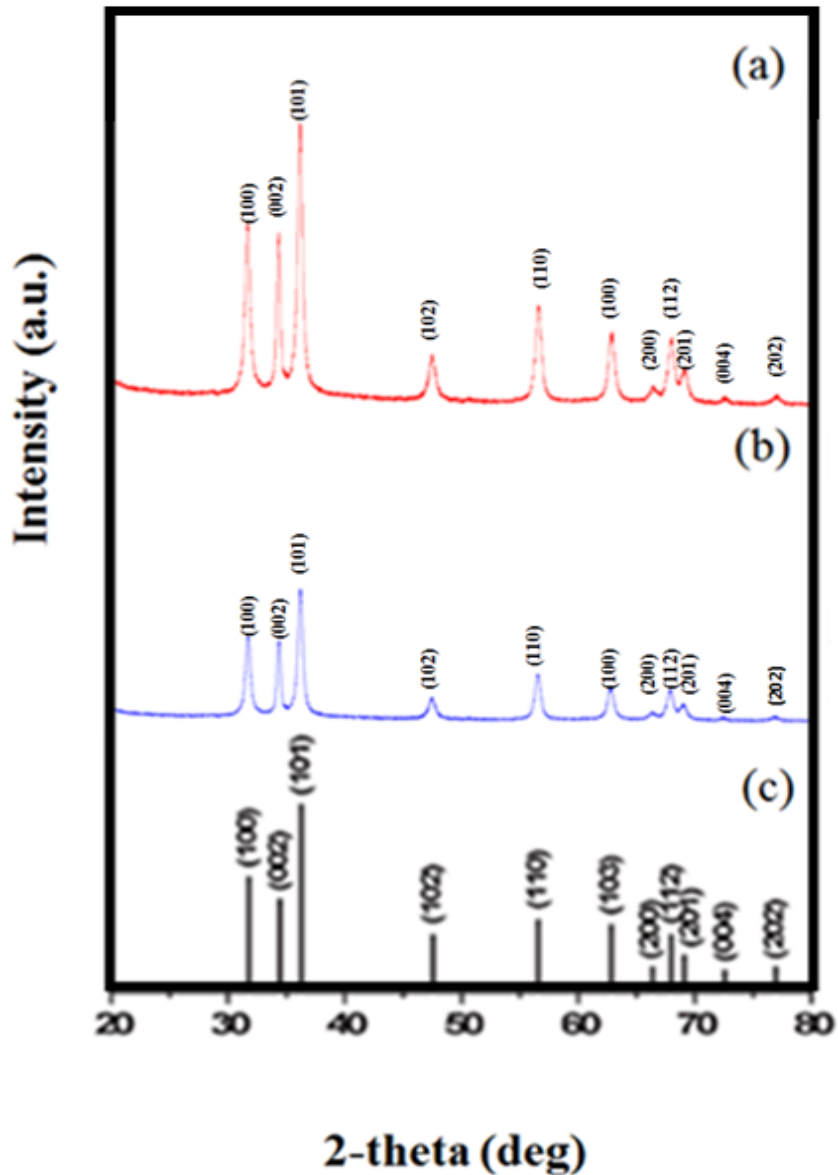


Figure 15. XRD of Zinc Oxide (a) Sample ZnO 1 (b) Sample ZnO 3 (c) JCPDS Reference

TEM Characterization

The morphology, size and microstructure of the synthesized zinc oxide nanoparticles were characterized by TEM using a Zeiss LIBRA TEM instrument operating at an accelerating voltage 120 kV. High-resolution images reveal **(Figure 16)** nanoparticles. Using ImageJ and Originpro the particle size distribution histogram **(Figure 16 b)** of zinc oxide sample 1 nanoparticles shows that the particle size ranges from 2-7 nm and possess an average size of 3.75 ± 0.57 nm. The structural features of the individual zinc oxide nanoparticles can be observed more clearly in the HR-TEM images. The optimum time of microwave irradiation **(Table 1)** was sample 4 **(Figure 16 d)** where the size of 15.8 nm was produced. The particle size increase at 20 minutes may attribute to agglomeration of smaller particles producing slightly larger particles under heat treatment.

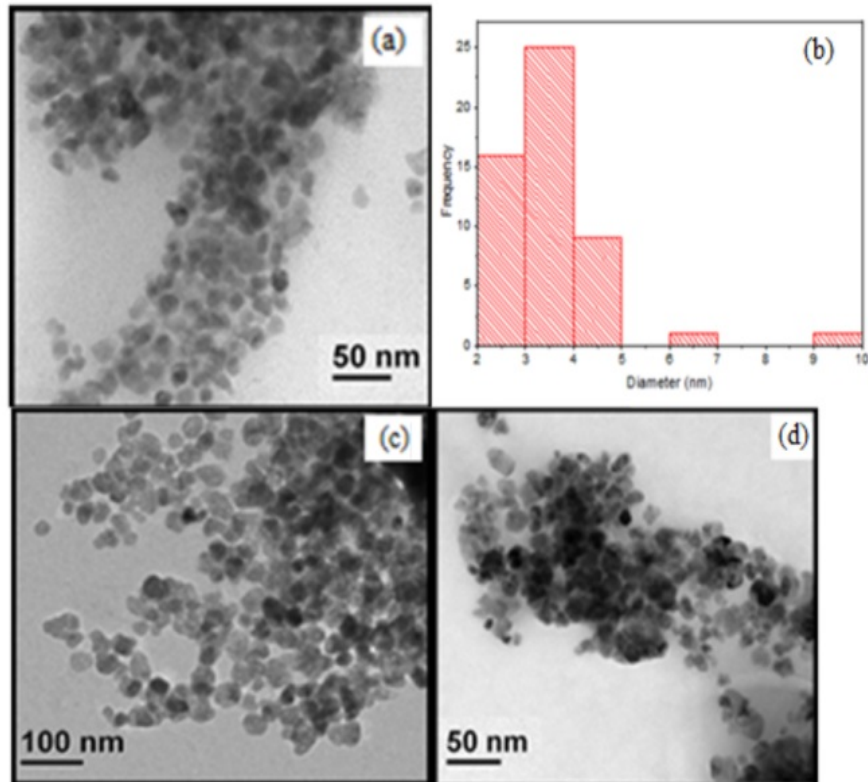


Figure 16. (a) TEM of ZnO Sample 1 (b) Particle Size Distribution Histogram of ZnO Sample 1 (c) TEM of ZnO Sample 3 (d) TEM ZnO Sample 4

LVEM5 Characterization

For comparison in **Figure 17** are the LVEM5 images of zinc oxide nanoparticles. The LVEM5 can measure particle size to capture the narrow size distribution. The operating parameters of a low voltage electron microscope produce resolutions that are not as high as the conventional TEM. Nevertheless, the advantages include an extremely small microscope and much greater image contrast because of the increased electron scattering. This suggests that staining is not needed for nanoparticle imaging therefore, reducing the electron transmittance and increasing contrast. Samples can be prepared reliably and reproducibly. **Figure 17** shows an example of an LVEM5 image of ZnO nanoparticles taken in TEM mode. **Figure 17c** is more

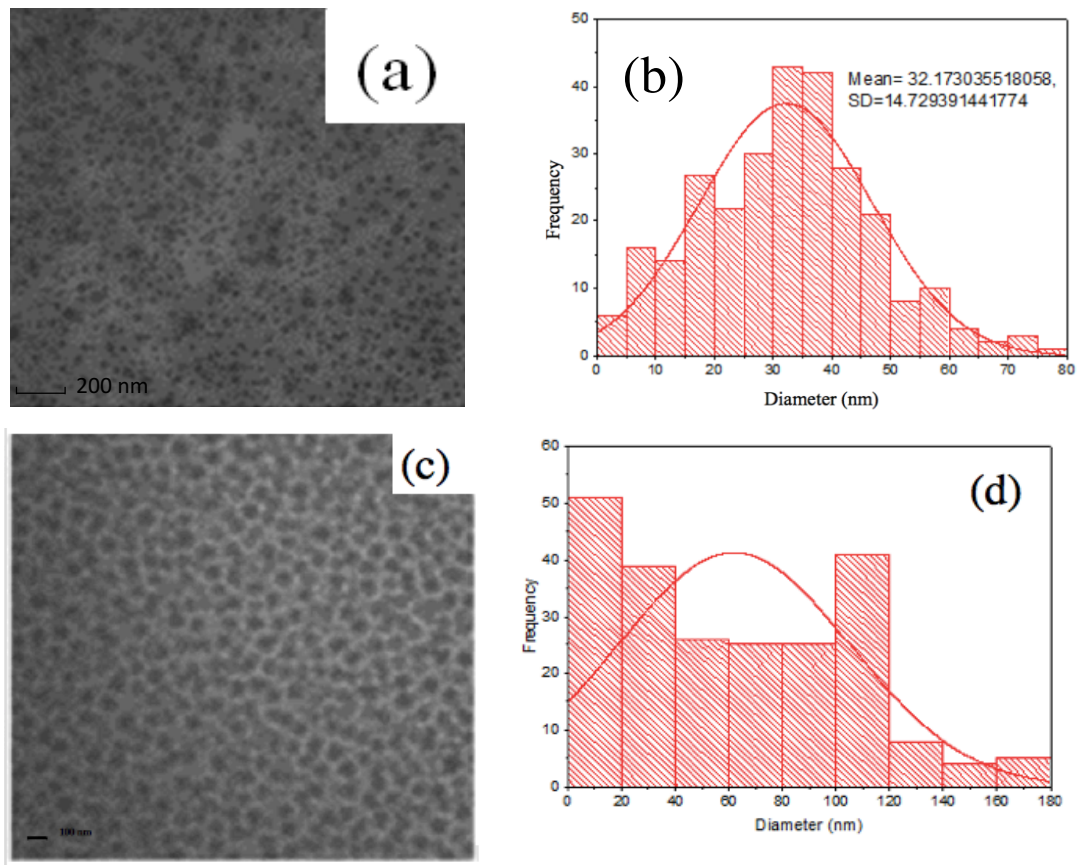


Figure 17. LVEM5 Images of Zinc Oxide Nanoparticles Taken at ~5kV in TEM mode (a) Conventional Synthesis of Zinc Oxide (b) Particle Size Distribution of The Conventionally Synthesized Zinc Oxide Nanoparticles (c) Microwave-Assisted Synthesis at 5 min (d) Sample 1 Histogram

aggregated than **Figure 17a** which is more distributed. The TEM images show zinc oxide nanoparticles of conventional synthesis (**Figure 17a**) and sample 1 of ZnO microwave-assisted synthesized nanoparticles (**Figure 17c**). Analyzing the image, average size of nanoparticles were estimated to be 32nm (**Figure 17b**). The size distribution of the nanoparticles due to growth after 60 min is shown in **Figure 17b** where a Gaussian curve is well-fitted to a frequency distribution histogram.

Optical Properties

Absorption spectrum of the zinc oxide nanoparticle solution obtained during a 30 minute reaction using the reference conditions outlined in the Experimental section are shown to absorb in the visible region (**Figure 18**). The energy gap is an essential characteristic in semiconductors and practical to applications in optoelectronics. These experiments were performed in order to understand the optical band gap, which was evaluated using

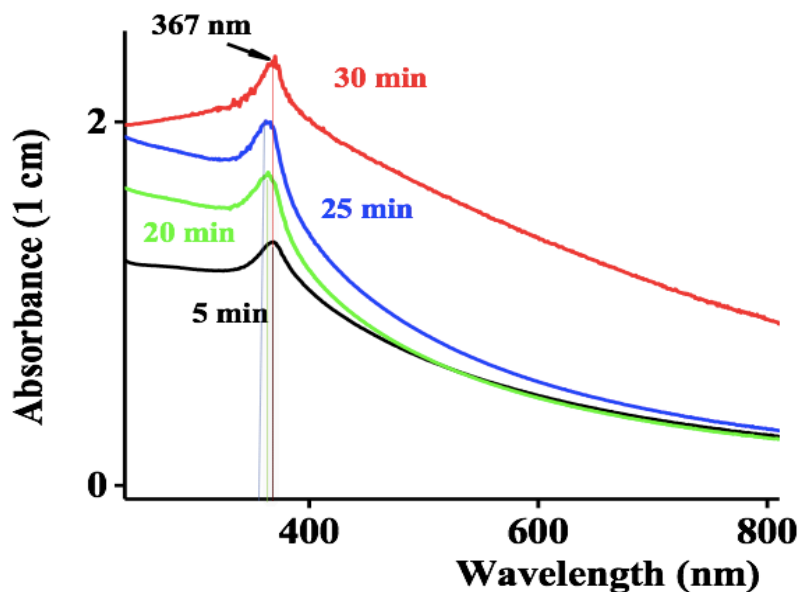


Figure 18. UV-Vis Absorption Spectra of Zinc Oxide

<http://instanano.com/characterization/theoretical/uv-vis-spectroscopy-band-gap-calculation/> as 3.38 eV. **Figure 18** shows the plot of the zinc oxide nanoparticles absorption at room temperature. The UV-Vis spectrum shows a sharp absorption band at 367 nm. The spectrum of ZnO nanoparticles depends on many parameters such as fabrication technique. The spectrum shifts toward the red region indicating that physical properties of the ZnO sample have changed.

FT-IR Characterization

Figure 19 shows the FT-IR spectrum of synthesized PVA-zinc oxide. The broad band located at 3297 cm^{-1} is the characteristic to the vibrational mode of O-H bond that corresponds to the PVA coating the zinc oxide nanoparticles. The peak of the C=O stretching of alcohol groups is located at 1600 cm^{-1} .

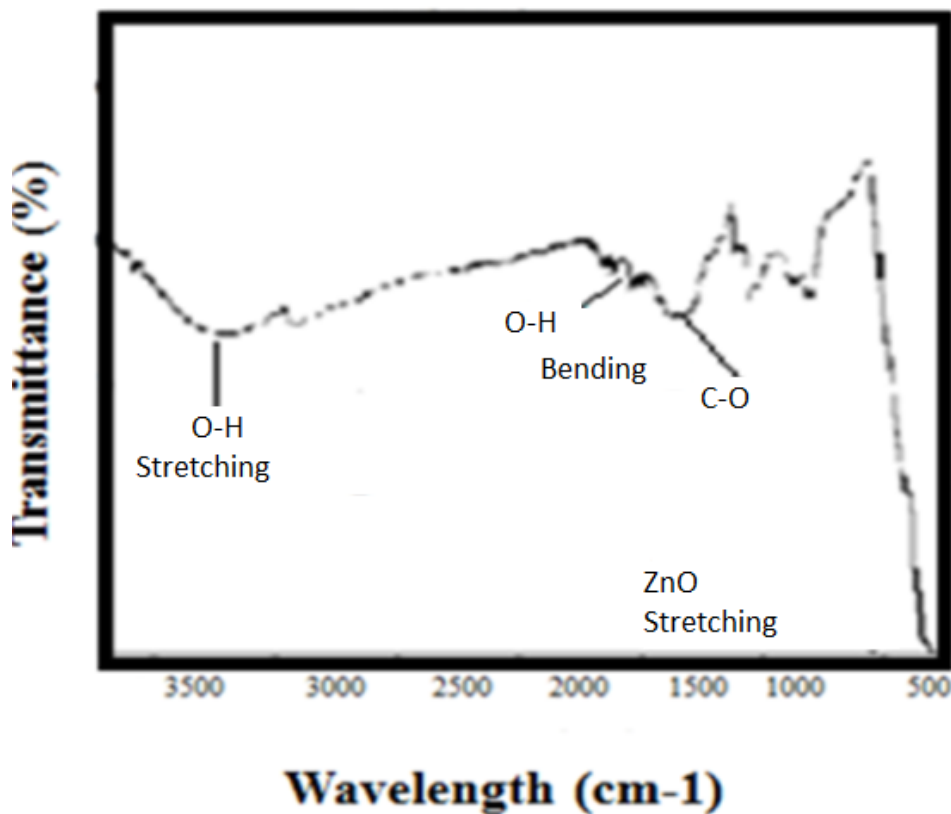


Figure 19. FT-IR of Zinc Oxide Nanoparticles

4.2 Characterization of In-House Synthesized Silver Nanoparticle

The synthetic methodology developed for typical in-house synthesized silver nanoparticles is described in the Experimental section along with their materials characterization methods. For in-house synthesized silver nanoparticles, absorptions and TEM micrographs were used to determine their successful synthesis. The absorption spectrum of silver nanoparticle solutions shows the conventional ~400 nm peak.

TEM micrographs show that silver nanoparticles prepared in an ice bath by chemical reduction are indirect evidence that capping limits Ostwald ripening (**Figure 20**). The citrate molecules attach to silver non-covalently to affect the size, growth, and increased concentration of the silver nanoparticles [168]. The formed ligands enable the high concentration compared to commercially available silver nanoparticles.

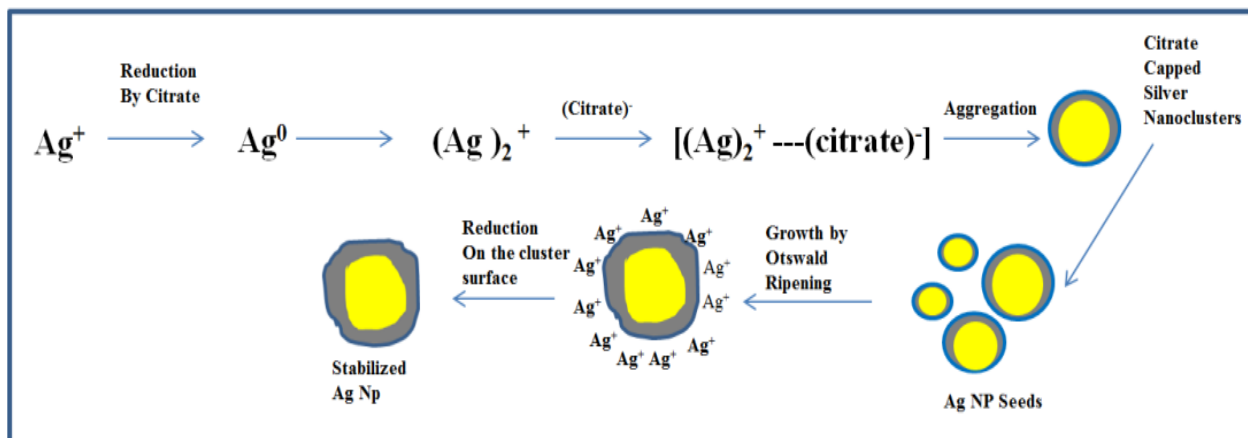


Figure 20. In-House Synthesized Silver Nanoparticles Growth Mechanism

In **Table 2** we show the design of experiments of the synthesized silver nanoparticles of diameters: 10 nm (sample 1), 9 nm (sample 2), 6.5 nm (sample 3), 5 nm (sample 4), 8.3 nm

(sample 5) and 16 nm (sample 6). Table 2. also shows the synthesized silver analyzed particle size and particle size distribution by TEM. Synthetic conditions impact silver nanoparticles size. The average core size of the silver nanoparticles as revealed by TEM was ~9 nm. All in-house synthesized silver nanoparticles exhibited a spherical morphology. The total concentration of the silver nanoparticle stock solution was 32.75 mg/mL. Following TEM investigation of the sample, the optical analysis of the particles is performed.

Table 2. Batch Synthesis Overview

Sample	Chemicals (g)			Reaction Conditions		
	FeSO ₄ ·7H ₂ O	C ₆ H ₅ Na ₃ O ₇ ·7H ₂ O	AgNO ₃	Time (min)	Nanopure H ₂ O (mL)	Average NP Size (nm)
1	9	18	3	10	120	10
2	9	18	1.5	10	120	9
3	9	18	3	5	120	6.5
4	9	18	1.5	5	120	5
5	9	18	3	20	120	8.3
6	9	18	3	2	120	16
7	9	18	3	30	120	ND
8	9	18	3	1	120	ND
9	9	18	1.5	1	120	ND
10	9	18	0.75	1	120	ND

ND: not determined

TEM Characterization

Diameter measurements of the in-house synthesized silver nanoparticles were obtained by TEM imaging on a Zeiss LIBRA 120 TEM. All of the synthesized silver nanoparticles were shown to have increased particle sizes compared to sample 4. The remaining silver sample solutions showed size increases between 1.5 nm and 5 nm, and size increases of 3 nm and 11 nm for the silver solution samples. Citrate has carboxyl groups which can be protonated and deprotonated depending on the pH. An increase from pH ~6 and 7 leads to the deprotonate form, $-\text{COO}^-$. The negatively charged carboxylate groups ($-\text{COO}^-$) of the surface bound molecules provide repulsion and prevent nanoparticles from aggregating immediately.

In **Figure 21** we show the TEM images of sample 1 through 6. TEM observations indicate that if the reaction is left to react for five minutes and half the amount of AgNO_3 , the resulting particles may range to approximately 5 nm (**Figure 21 a**) and the shape and size distribution of the particles are highly monodispersed.

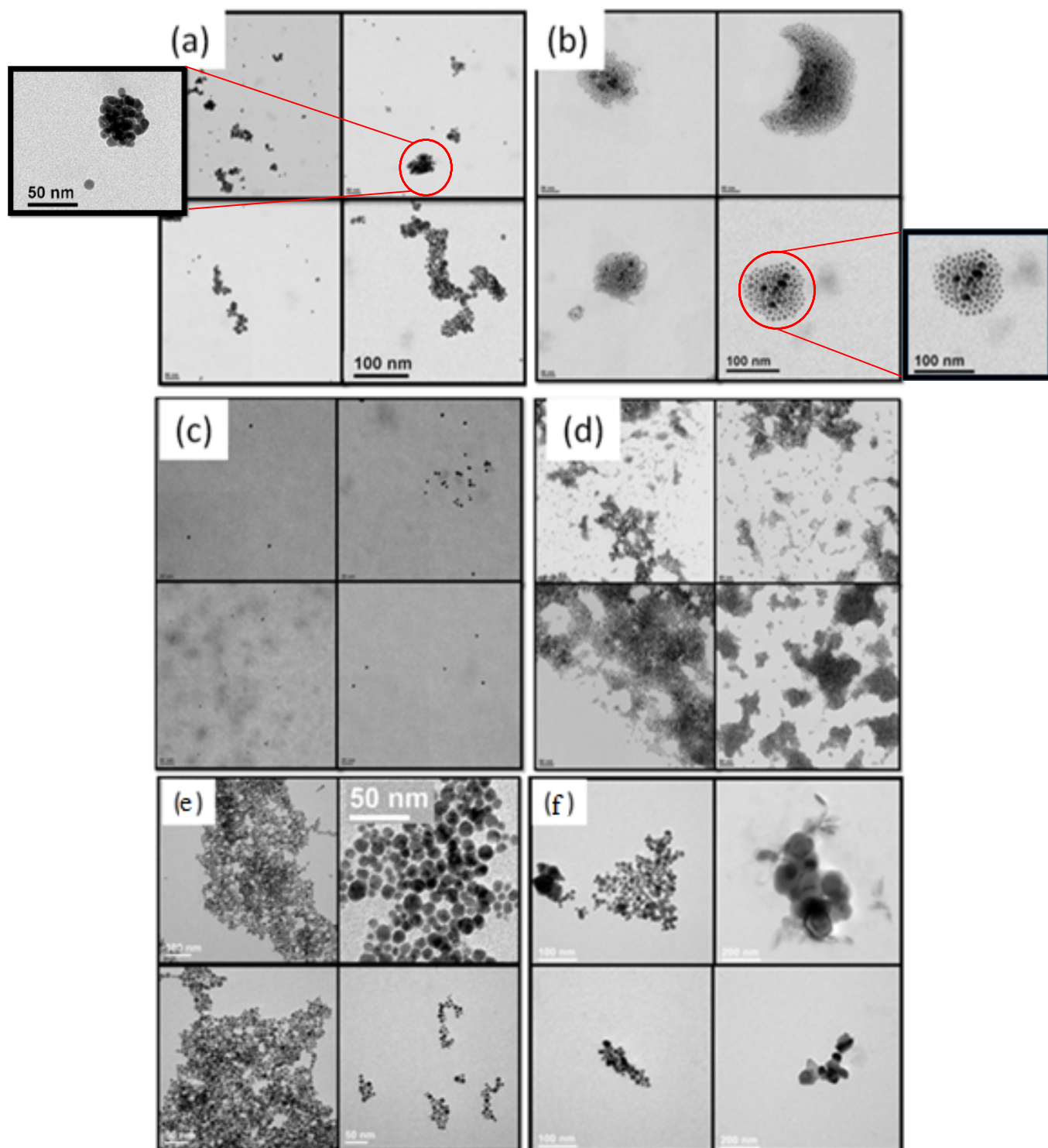


Figure 21. HRTEM of Synthesized Silver Nanoparticles (a) Sample Ag 1 (b) Sample Ag 2 (c) Sample Ag 3 (d) Sample Ag 4 (e) Sample Ag 5 and (f) Sample Ag 6

LVEM5 Characterization

The TEM images were captured using an LVEM5 electron microscope at an operating voltage ~ 5 kV as an exceptional method to quickly characterize nanoparticles. The low voltage permits direct imaging without sample staining. **Figure 22** were captured at highest resolution enabled by this instrument. Scanning electron microscopy (SEM) images of the as-synthesized silver nanoparticle solution samples were taken directly (without any coating of conductive material) with a LVEM5 5 kV microscope. The size, shape, morphology and distribution of the synthesized silver nanoparticle solutions were examined by TEM. In addition, SEM was used as a complementary technique to examine the silver nanoparticles (**Figure 22**).

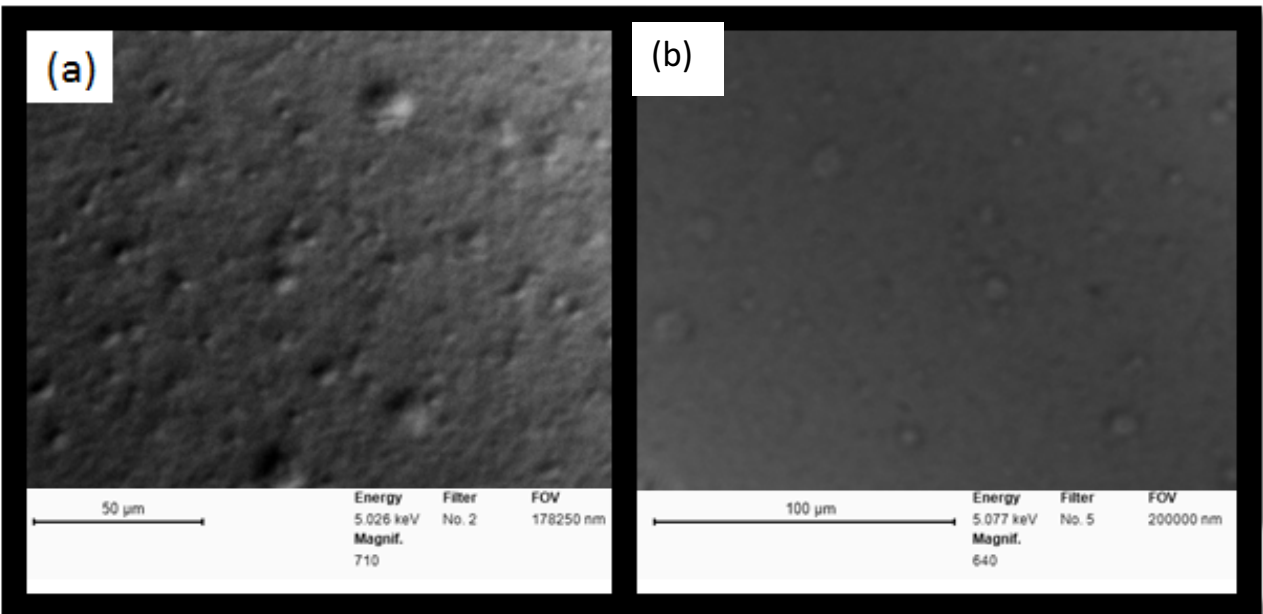


Figure 22. (a) Low Voltage SEM Sample Ag 1 (b) SEM Sample Ag 1 At Lower Magnification

Optical Properties of Synthesized Silver

The optical properties of silver nanoparticles can change depending on size, shape, composition and surface capping around the nanoparticle [169]. The absorbance values (**Figure 23**) and TEM diameters (**Table 2**) of the citrate capped synthesized silver nanoparticles were measured. We show the absorbance spectra of synthesized silver nanoparticles of 10 nm (sample 1). The absorbance spectra of the prepared silver nanoparticle solutions showed an absorption band at ~400 nm as shown in **Figure 23a**. This is a typical absorption band of spherical silver nanoparticles with a diameter smaller than 100 nm. The concentrated silver solution was tested by observing its absorption spectrum after diluting 100 times.

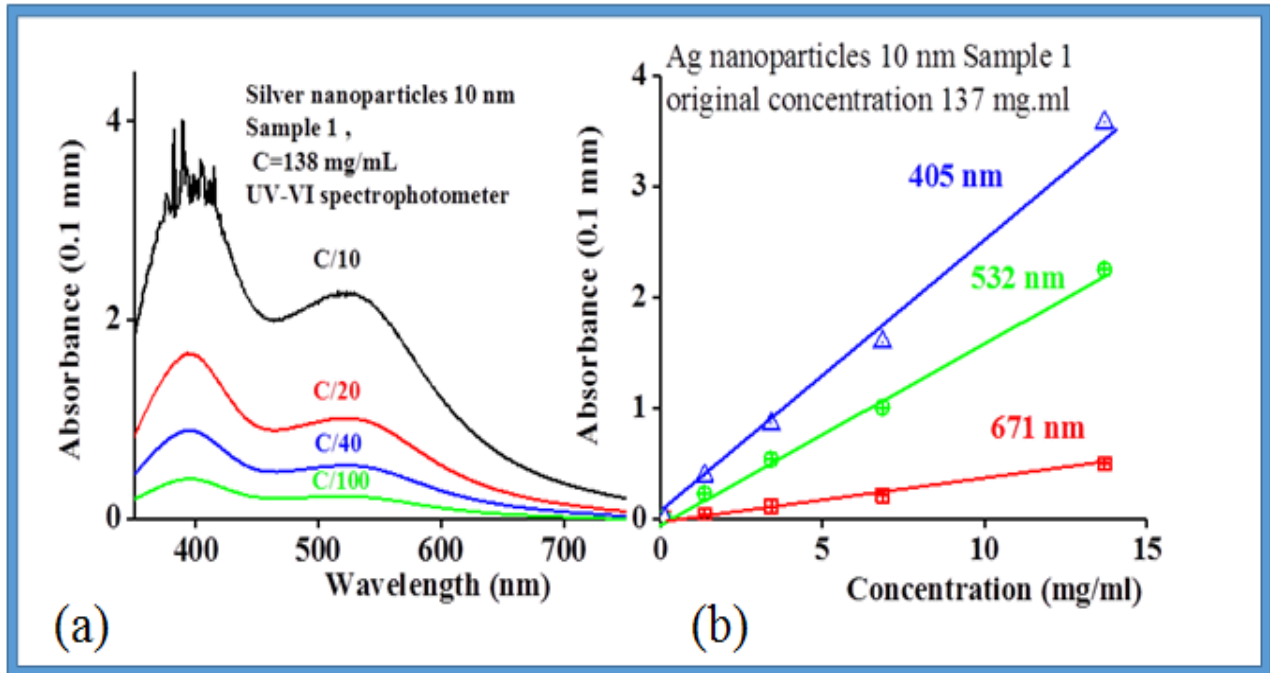


Figure 23. (a) Absorbance of Synthesized Silver Nanoparticles (b) Absorbance of Silver Nanoparticles as A Function of Concentration

The absorption spectrum of the diluted silver nanoparticle solutions show indistinguishable spectral features to the spectrum of the original solution of silver nanoparticles. This validates that the synthesized silver nanoparticles are not agglomerated. Obviously, there are two absorption bands (**Figure 23 a**) at about 400 nm and 525 nm. The two peaks are an interesting effect of the plasmon resonance. The dipole approximation is associated with the primary peak and quadrupole and Mie approximation is associated with the secondary peak.

Optical measurements of in-house synthesized silver nanoparticles suggest that ligand capped silver nanoparticles increase the concentration of silver nanofluid and follow Beer's Law at low and high concentrations. **Figure 23 (b)** is the absorbance spectra of diluted synthesized silver nanoparticles for three wavelengths: 405, 532, and 671 nm and further confirms that aggregation in synthesized silver nanoparticle solution is not observed suggesting that the concentrated sample remained stable. To determine how strongly the synthesized silver nanoparticles absorb light at 405 nm, the Beer-Lambert law can be used to calculate the

$$A = \epsilon cl \quad (13)$$

And can be rewritten in terms of ϵ .

$$\epsilon = A/lc \quad (14)$$

molar absorptivity from the sample's absorbance spectrum. Using a cuvette with a length of 0.1 mm, a molar concentration of 0.30 mol/L and the absorbance at wavelength 405 nm is 1.75. The molar absorptivity of the solution is $58 \text{ L mol}^{-1} \text{ cm}^{-1}$.

4.3 Characterization of Commercially Available Silver Nanoparticle

Optical Properties

The characteristic colors (**Figure 24**) of Nanocomposix colloidal silver nanoparticle solutions are a result of a phenomenon known as plasmon absorbance. Electromagnetic radiation is absorbed on the surface of nanoparticles when incident light oscillates in conduction electrons.

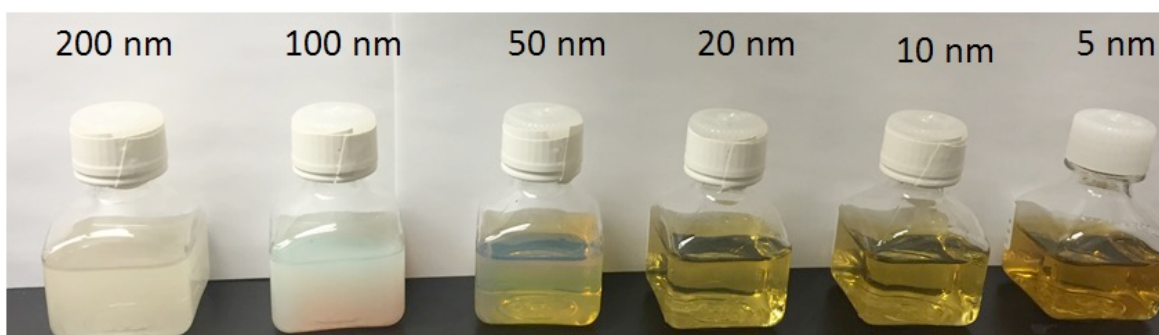


Figure 24. Nanocomposix Colloidal Solutions of Various Silver Nanoparticle Size

Using a 1 cm pathlength cell the absorbance of the commercially available silver nanoparticles were measured and show a pronounced peak at ~ 400 nm (**Figure 25**). Smaller Ag nanoparticles exhibit a peak at 400 nm. The interaction with light and electrons on the surface of the silver nanoparticles oscillate their specific wavelengths allowing high wavelengths. As the particle size increases the absorbance peak increases and broadens due to increased scattering. The curve shifts toward the red region for particles above 100 nm, a second band at lower wavelength becomes obvious due to quadrupole resonance as well as the primary dipole resonance.

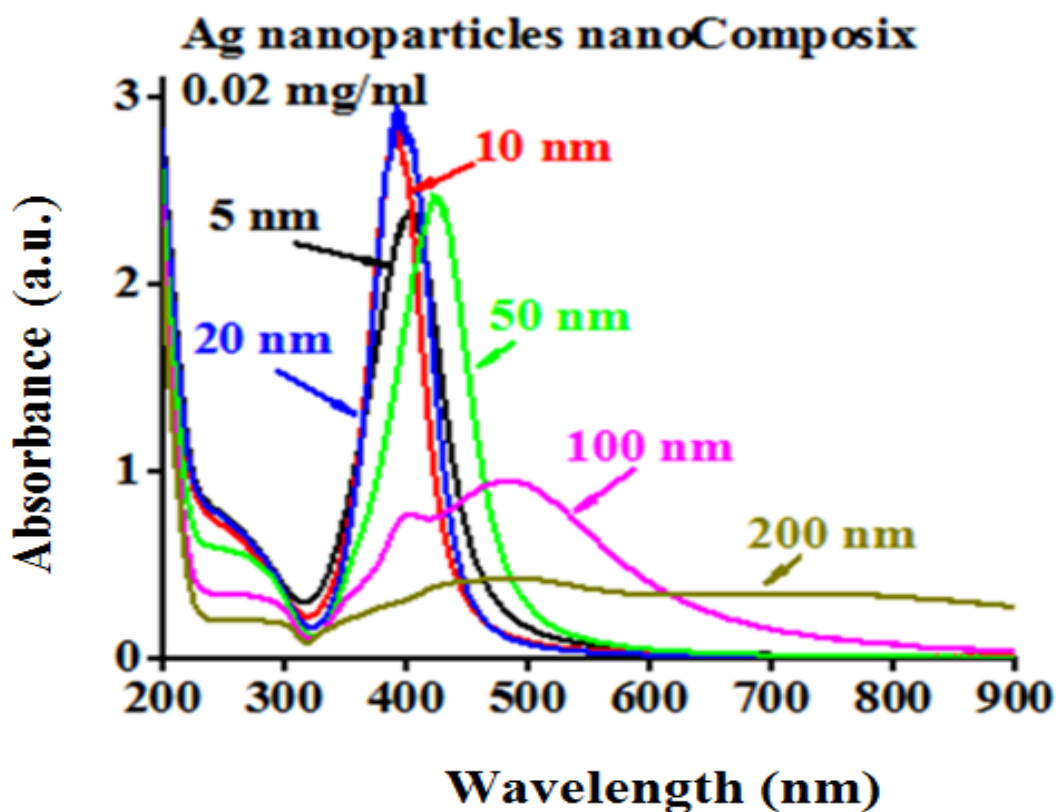


Figure 25. UV-Vis Absorbance of Nanocomposix Nanoparticles as A Function of Size

TEM Characterization

The TEM images obtained from Nanocomposix of commercially available silver

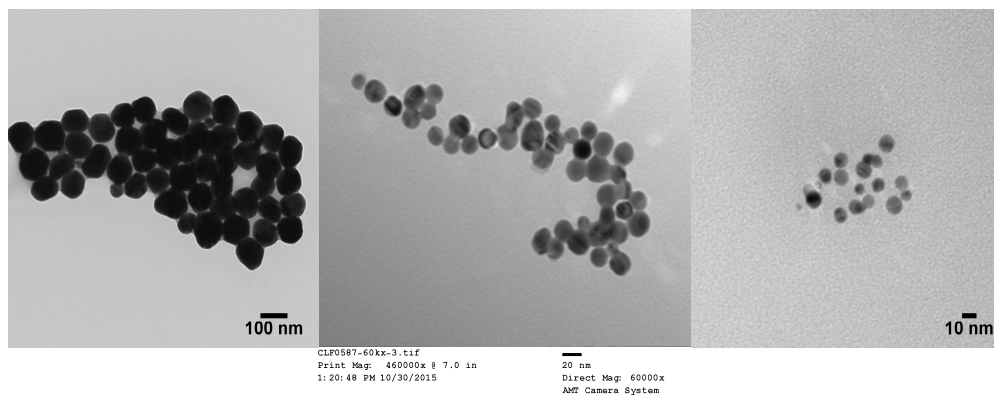


Figure 26. HRTEM of Nanocomposix Silver Nanoparticles (Used with permission from Nanocomposix [170])

nanoparticles solutions in **Figure 26** [170] were captured on a JEOL 1010 TEM and indicate that the larger particles plasmon peak shifts to longer wavelengths and broadens.

PTL Characterization

To perform PTL experiments (**Figure 27**) a 0.1 cm pathlength cell is used. We show that the extinction was found to follow a third order dependence with the diameter of the particles because of scattering. For larger silver nanoparticles, we show a sixth order dependence.

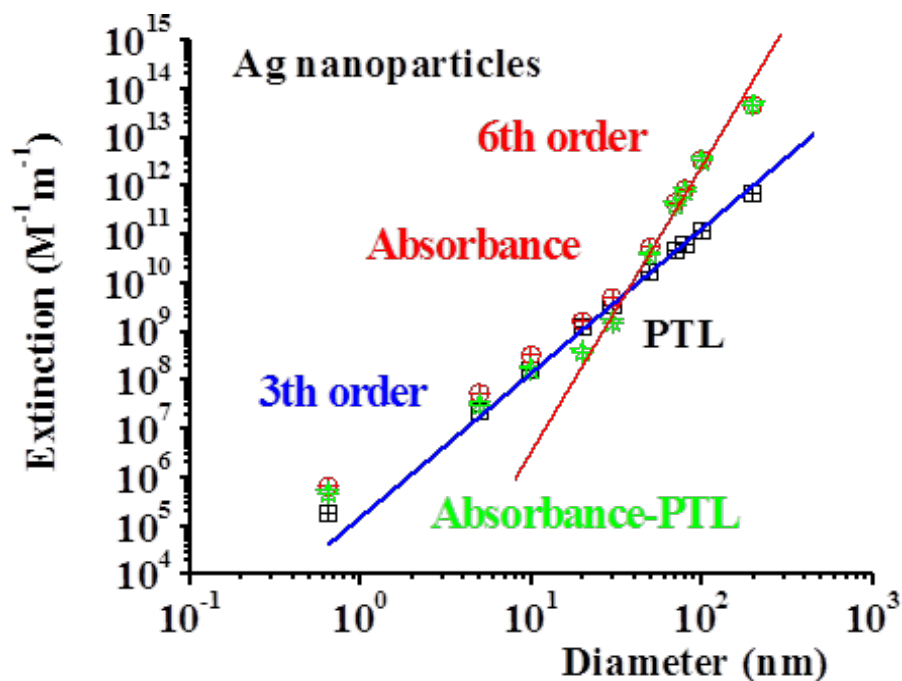


Figure 27. PTL Spectra of Nanocomposix Nanoparticles

Absorbance and PTL experiments were performed to determine the extinction, how strongly the Ag nanoparticles absorb light, as well as the absorption and scattering cross-section values of Ag

NPs of different dimensions. We show that the extinction cross-section obtained from the absorbance experiment depends on the cube of the particle's diameter for particles of a diameter smaller than 70 nm. For larger particles a sixth order dependence becomes evident in the spectral regions far from the plasmonic peak in the region of 400 nm. The cross-section obtained using the PTL method confirms the absorption character of the signal without contribution from scattering effects. The results are in agreement with the basic Rayleigh model of absorption and scattering of small particles. Based on the observations we establish empirical equations for the determination of the absorption and scattering cross-section values of the nanoparticles.

CHAPTER 5. CONCLUSION

Nanoparticles are becoming ubiquitous nowadays' in consumer products. Despite their increased popularity, the assessment of their potential hazards is far from exhaustive. Synthetic conditions of these products are typically harsh, requiring high temperatures and render low yields. In this thesis, it was shown that such reaction conditions could be dramatically improved through energy efficient, sustainable approaches. The most common occurrence of nanoparticles in consumer products is in electronics, food, cosmetics, and cleaning products. Two categories were selected, metal and metal oxides, to demonstrate sustainable nontoxic, sustainable and energy efficient synthetic conditions.

5.1 Summary of Research Findings of Zinc Oxide Nanoparticle

Zinc oxide nanomaterials were synthesized at low temperatures by microwave-assisted synthesis in nanopure water. The materials were characterized for optical properties. These measurements provided a band gap of 3.38 eV at ambient temperatures (calculated by UV-Vis) attributing to semiconductor characteristics.

Nanoparticles naturally aggregate, therefore, surfactants (or capping agents) are employed to prevent aggregation. In the case of ZnO, poly(vinyl alcohol) (PVA) capping ligands are still present on the surface and evident by FT-IR spectroscopy (showing a strong peak of O-H). In the FT-IR spectra of PVA-ZnO, the main peak detected at 3970 cm^{-1} is assigned to the O-H stretching vibration of the hydroxyl group.

5.1.1 Summary of Research Findings of Synthesized Silver Nanoparticle

Silver nanoparticles are synthesized and used for a wide range of applications from electronics to agriculture. A novel procedure is presented of silver nanoparticles that provides high concentrations, which can qualify the resulting dispersions as nanofluids. In comparison, commercially available silver nanoparticles are low in concentration. Silver nanoparticle dispersions, highly stability, were amenable to thin film preparation, as a demonstration of their potential usefulness in consumer electronics. Thin-films, prepared by a simple spin-coating and spray coating process, followed by plasma treating, showed enhanced conductivity.

5.1.2 Summary of Research Findings of Commercially Available Silver Nanoparticles

The absorbance experiments of commercially available silver nanoparticle solution determined the extinction, absorption and scattering cross-section values of the silver nanoparticles as a function of its diameter. From the absorbance, we were able to show that the particle size of smaller than 70 nm exhibit scattering and depends on the cube of its diameter. Whereas, silver nanoparticles larger than 70 nm depends on the sixth order of the particle's diameter. The absorbance experimental results were confirmed using PTL method which does not include the scattering contributions.

The experiments have shown that the particles synthesized by the experimental approach described in this thesis are similar to the commercially available ones.

5.2 Final Conclusions

5.2.1 Zinc Oxide Nanoparticles Synthesis

It has been shown that the microwave-assisted synthesis method offers a simple methodology at low temperatures and short reaction time. Low temperature synthesis of zinc oxide nanoparticles starting from zinc acetate dehydrate, PVA, and sodium hydroxide in nanopure water was performed via microwave-assisted synthesis. The nanoparticles were characterized through, TEM, X-ray diffraction, FT-IR, and UV-Vis. TEM was regularly used for imaging nanoparticle size and size distribution. FT-IR enabled the identification of molecules present of the surface. To analyze optoelectronic properties UV-Vis techniques were used. To identify crystalline phases in zinc oxide nanoparticles the use of X-ray diffraction techniques was employed. The XRD study indicates a hexagonal wurtzite zinc oxide nanostructure. The microwave-assisted synthesis method does not require difficult treatments or high-priced chemicals demonstrating its advantage over other techniques. It is also concluded that nanoparticle synthesis by microwave-assisted synthesis is consistent with solvothermal synthesis. The success of the method may influence further studies to explain pulsating microwaves and the microwave synthesis of other materials. These perspectives may be considered in the synthesis of other inorganic microwave- assisted syntheses of nanoparticles in aqueous solution.

5.2.2 Synthesized Silver Nanoparticles Synthesis

Well-distributed silver nanoparticle solutions were synthesized in an ice bath via a chemical reduction method. At a controlled temperature, the formation of highly distributed

silver nanoparticles was observed by varying reaction times and initial concentrations of metal salt. The silver nanoparticle synthesis was further studied by varying reaction times and keeping concentrations of silver nitrate constant. Following this, the concentrations of silver nitrate were held constant while varying the reaction times. The reaction times of 10 minute for sample 1 and sample 2 were found to have a significant effect on the formation of stable silver nanoparticle materials of 9 nm and 10 nm. Nanoparticles in sample 3 and sample 4 range between 5 nm and 6.5 nm. These measurements were obtained 5 minutes after the reaction proceeded. However, the reaction times of the same samples were not consistent with results of varying the concentrations of silver nitrate. This observation suggests that the occurrence of nanoparticles of 6.5 nm to 5 nm is controlled by the duration of the reaction and not the initial concentration of silver nitrate.

The absorbance of the silver nanoparticles was observed at 400 nm. It was found that the formation and size control of silver nanoparticle size decreased with decreasing starting materials concentration. However, the average diameter of silver nanoparticles increased with increasing reaction time. Silver nanoparticle growth appeared to be kinetically guided as seen by a low concentration of metallic salt followed by the concentration of trisodium citrate: pH 7.5-9. Therefore, chemical reduction method for the synthesis of silver particles with a diameter of 5 nm, is achieved by decreasing the reaction time and reducing the amount of silver salt precursor. Absorbance data of silver nanoparticle solution showed that the highly concentrated sample did not exhibit aggregation. Therefore, this is an efficient, eco-friendly and simple method for highly stable silver nanoparticles. The silver nanoparticle solutions were also prepared for films and deposited via spin and spray coating.

5.3 Discussion

Nontoxic routes are discussed for the synthesis of zinc oxide nanoparticles and silver nanoparticles. By comparison, different methods and particle size produced from previous reports use high temperatures or toxic solvents. The synthesis approach described in this thesis is superior because the formation of nanoparticles entails that a narrow size distribution, in nanopure water as a solvent is possible.

5.3.1 Discussion of Zinc Oxide Nanoparticles

Our microwave-assisted green chemistry approach for the nontoxic synthesis of PVA capped zinc oxide nanoparticles could be the promising potential. In the past, microwave synthesis of zinc oxide has been studied by several authors suggesting the use of a domestic microwave where the temperature cannot be controlled or harsh products where the potential risks can negatively impact the user or the environment. Reports argue that the use of these techniques increases the chances of successful nanoparticle synthesis. However, it was reported that the zinc oxide nanoparticle synthesis was in fact enhanced because of the avoidance of toxic chemicals and high reaction temperatures.

5.3.2 Discussion of Synthesized Silver Nanoparticles

The synthesis and characterization of their different size, morphology, and size distribution were investigated. The effect of the initial concentrations of the precursor, silver nitrate and the reaction times demonstrate the wide range of silver nanoparticle size attainable.

The procedure described here offers better particle size and more concentrated silver nanoparticles at low temperatures.

5.4 Suggestion for Future Research

Suggestions for Future Research Regarding Zinc Oxide Nanoparticles

Zinc oxide nanoparticles have been used for cosmetics, photovoltaics, and transparent conductors. Microwave-assisted synthesis has many advantages such as fast crystallization and short reaction times compared with conventional heating. Future studies will focus on tailoring the microwave parameters as well as exploring the procedures prior to microwave synthesis to eliminate unnecessary steps.

Suggestions for Future Research Regarding Synthesized Silver Nanoparticles

Recommendation for future research include producing and characterizing nanoparticles for nanofluids. Additionally, work is needed to develop coating methods that are scalable and are industry compatible to meet the needs for films with a larger size.

5.5 Technological Applications of ZnO and Ag Nanoparticles

Throughout the world the production of environmentally safe and energy efficient materials is essential, and nanoparticles' role in new technologies and new products is constantly increasing. The focus of this research was on the green and energy saving synthesis routes for

ZnO NPs and Ag NPs. As mentioned previously, our technology-driven society commonly exploits NPs' intrinsic properties for numerous industrial processes and consumer products. For instance, a photovoltaic device generating electricity by the direct conversion of sunlight involves both a physical and a chemical phenomenon and to optimize such device, one could act in both directions. Use of nanoparticles in renewable energy devices impacts both the chemistry, through composition and surface chemistry, and the physics, by morphology, size, and optoelectronic properties derived from these dimensionalities, along with overall device physics.

From the data collected in this work, in-house synthesized Ag NPs or ZnO NPs are appealing materials for a variety of applications ranging from photovoltaic technologies, pharmaceuticals, nanocomposites, electronics (conductive inks, semiconductors), and catalysis for energy conversion and storage. To synthesize nanoparticles, we introduced less toxic methods of two commonly used nanomaterials, ZnO and Ag.

ZnO

Attractive features of ZnO nanomaterial are that it is low in cost, non-toxic and it can be doped with elements like Al to enhance its semiconductor properties, potentially, creating faster, more efficient, and cost-effective semiconductors. Additionally, technological applications of ZnO NPs further expanded to cosmetic powders, food packaging, antibacterial, drug delivery. The later emerging applications relate to the finding of antibacterial properties in ZnO NPs.

ZnO potential in several applications could be limited by the ability to produce large quantities with energy saving processes, high yields and fast reaction times. Improvement of these parameters is essential to expanding the technological applications of this useful material.

We have developed a green approach for nano-scaled ZnO particles using an eco-friendly microwave-assisted synthesis method as an alternative method. This method is faster, reproducible, and uses water as a solvent. ZnO NPs can be made quickly, at low temperatures without the use of toxic solvents. We could accelerate the chemical reaction performed by microwaves in an isolated-airtight-vessel as well as control the pressure and temperature to achieve controlled growth of ZnO NPs. The microwave reactions are appealing because of the potential for inexpensive, and time sufficient growth of NPs.

Based on our results, microwave technology speeds up industrial processes and increases the yield of our in-house synthesized ZnO NPs. The recent discovery of ZnO NPs' antibacterial properties reveals that our experimental approach of using eco-friendly microwave-assisted synthesis as a powerful emerging technique to synthesize nanoparticles is non-toxic and is FDA approved.

Ag

In the past decade, the number of technological applications involving Ag NPs have been rocketing; products have been introduced to the market in increasing amounts. For example, in the medical field, applications span from antibacterial products, initial stage of clinical trials in cancer therapy, drug delivery, to cell imaging and bioengineering. The use of Ag NPs significantly improves the healing process of wounds and its use as an anti-inflammatory and antibacterial agent stimulate body repairs. Adding Ag NPs to disinfectant solutions and antibiotics is commonly used for killing germs. This drove to expanding their usefulness to

modern textile industries and other consumer goods such as paint products, kitchenware, and toys which contain Ag NPs in order to prevent bacteria and mold.

However, all the above applications require low concentrations of Ag NPs. Silver application the electronics industry, photovoltaic technologies, semiconductors and catalysis include conductive inks, pastes, inkjet, and screen-printing for integrated circuits. Therefore, large quantities need to be produced.

When introducing inks formed of Ag NPs, findings indicate that efficient applications require not only the quantity but also NP characteristics such specific diameters of the Ag NPs, to prevent blockage in the nozzle and to ensure fluidity. In addition, the use of water as carrier medium is highly recommended as means of decreasing toxicity of the approach. The disadvantage of existing synthetic methods for Ag NPs inks is that they utilize potentially hazardous chemicals, often require high temperature in NPs preparation, create toxic byproducts, and generate a lot of hazardous waste.

More recently, the desire to increase efficiency in heat transfer processes also indicated that a highly concentrated colloid (nanofluid) with high thermal conductivity would be an appealing pathway.

In this study, we presented a new method to synthesize a highly concentrated Ag NP nanofluid, which is prepared in truly benign conditions (nanopure water using sodium citrate through a chemical reduction method). The in-house synthesized Ag nanofluids are superior to commercially available Ag NP solutions, which are typically produced at very low concentrations with expensive methodologies. As explained in this thesis, the in-house

synthesized Ag NPs are very high in concentration, and suitable both in future nanofluid technology applications as well as in conductive inks for electronics.

REFERENCES

- [1] Yung LC, Fei CC, Mandeep J, Binti Abdullah H, Wee LK. Synthesis of a nano-silver metal ink for use in thick conductive film fabrication applied on a semiconductor package. *PLoS One* 2014;9:e97484. doi:10.1371/journal.pone.0097484.
- [2] Bi XY, Westerhoff P. Adsorption of iii/v Ions (In(iii), Ga(iii) and As(v)) onto SiO₂, CeO₂ and Al₂O₃ Nanoparticles Used In the Semiconductor Industry. *Environ Sci Nano* 2016;3:1014–26. doi:10.1039/C6EN00184J.
- [3] Zhong L-S, Hu J-S, Liang H-P, Cao A-M, Song W-G, Wan L-J. Self-Assembled 3D Flowerlike Iron Oxide Nanostructures and Their Application in Water Treatment. *Adv Mater* 2006;18:2426–31. doi:10.1002/adma.200600504.
- [4] Hamers RJ. Nanomaterials and Global Sustainability. *Acc Chem Res* 2017;50:633–7. doi:10.1021/acs.accounts.6b00634.
- [5] Hamers RJ, Tromp RM, Demuth JE. Surface Electronic Structure of Si (111)-(7x7) Resolved in Real Space. *Phys Rev Lett* 1986;56:1972–5. doi:10.1103/PhysRevLett.56.1972.
- [6] Murray CB, Norris DJ, Bawendi MG. Synthesis and Characterization of Nearly Monodisperse CdE (E= S, Se, Te) Semiconductor Nanocrystallites. *J Am Chem Soc* 1993;115:8706–15. doi:10.1021/ja00072a025.
- [7] Alivisatos AP. Semiconductor Clusters, Nanocrystals, and Quantum Dots. *Science* (80-) 1996;271:933–7.
- [8] Bruce PG, Scrosati B, Tarascon J-M. Nanomaterials for rechargeable lithium batteries. *Angew Chem Int Ed* 2008;47:2930–46. doi:10.1002/anie.200702505.
- [9] Elmer WH, White JC. The Use of Metallic Oxide Nanoparticles to Enhance Growth of Tomatoes and Eggplants in Disease Infested Soil or Soilless Medium. *Environ Sci Nano* 2016;3:1072–9. doi:10.1039/C6EN00146G.
- [10] Khot LR, Sankaran S, Maja JM, Ehsani R, Schuster EW. Applications of nanomaterials in agricultural production and crop protection: A review. *Crop Prot* 2012;35:64–70. doi:https://doi.org/10.1016/j.cropro.2012.01.007.
- [11] Feynman RP. There's plenty of room at the bottom. *Eng Sci* 1960;23:22–36.
- [12] Nielsen AE. Kinetics of precipitation. vol. 350. Pergamon Press Oxford; 1964.
- [13] Ring TA. Fundamentals of Ceramic Powder Processing and Synthesis. San Diego, Calif: Academic Press; 1996.
- [14] Cushing BL, Kolesnichenko VL, O'Connor CJ. Recent Advances in the Liquid-Phase Syntheses of Inorganic Nanoparticles. *Chem Rev* 2004;104:3893–946.

doi:10.1021/cr030027b.

- [15] Dirksen JA, Ring TA. Fundamentals of crystallization: Kinetic effects on particle size distributions and morphology. *Chem Eng Sci* 1991;46:2389–427. doi:10.1016/0009-2509(91)80035-W.
- [16] TROMP RM, HANNON JB. THERMODYNAMICS OF NUCLEATION AND GROWTH. *Surf Rev Lett* 2002;9:1565–93. doi:10.1142/S0218625X02003846.
- [17] Myerson AS. *Handbook of Industrial Crystallization*. vol. 2nd ed. Boston: Butterworth-Heinemann; 2002.
- [18] Lifshitz IM, Slyozov VV. The kinetics of precipitation from supersaturated solid solutions. *J Phys Chem Solids* 1961;19:35–50. doi:10.1016/0022-3697(61)90054-3.
- [19] Yonezawa T, Onoue S, Kimizuka N. Preparation of Highly Positively Charged Silver Nanoballs and Their Stability. *Langmuir* 2000;16:5218–20. doi:10.1021/la000186f.
- [20] Pastoriza-Santos I, Liz-Marzán LM. Formation and Stabilization of Silver Nanoparticles through Reduction by N,N-Dimethylformamide. *Langmuir* 1999;15:948–51. doi:10.1021/la980984u.
- [21] Fievet F, Lagier JP, Figlarz M. Preparing Monodisperse Metal Powders in Micrometer and Submicrometer Sizes by the Polyol Process. *MRS Bull* 1989;14:29–34. doi:DOI: 10.1557/S0883769400060930.
- [22] Yu W, Tu W, Liu H. Synthesis of Nanoscale Platinum Colloids by Microwave Dielectric Heating. *Langmuir* 1999;15:6–9. doi:10.1021/la9806505.
- [23] Tsuji M, Hashimoto M, Tsuji T. Nucleation, Fast Preparation of Nano-sized Nickel Particles under Microwave Irradiation without Using Catalyst for. *Chem Lett* 2002;31.
- [24] Tu W, Liu H. Continuous Synthesis of Colloidal Metal Nanoclusters by Microwave Irradiation. *Chem Mater* 2000;12:564–7. doi:10.1021/cm990637l.
- [25] Zhu J, Palchik O, Chen S, Gedanken A. Microwave Assisted Preparation of CdSe, PbSe, and Cu_{2-x}Se Nanoparticles. *J Phys Chem B* 2000;104:7344–7. doi:10.1021/jp001488t.
- [26] Brinker CJ, Scherer GW. *Sol-gel science: the physics and chemistry of sol-gel processing*. Academic press; 2013.
- [27] Pierre AC. *Introduction to Sol–Gel Processing* Kluwer International Series in Sol–Gel Processing: Technology and Applications 1998.
- [28] Sakka S. *Sol-Gel Science and Technology: Topics in Fundamental Research and Applications (4 Volume Set)*. Taylor & Francis US; 2002.
- [29] Tokumoto MS, Pulcinelli SH, Santilli C V, Briois V. Catalysis and Temperature Dependence on the Formation of ZnO Nanoparticles and of Zinc Acetate Derivatives Prepared by the Sol–Gel Route. *J Phys Chem B* 2003;107:568–74.

doi:10.1021/jp0217381.

- [30] Pechini M. Method of preparing lead and alkaline earth titanates and niobates and coating method using the same to form a capacitor 1967.
- [31] 1963, Ser. Method of Preparing Lead and Alkaline Earth Titanates and Niobate\$ and Coating Method Using the Same To Form a Capacitor, 1967.
- [32] Chiang C, Shei CY, Wu SF, Huang YT. Preparation of high-purity Tl-based “1223” superconductor phase by modified Pechini process in water solution. *Appl Phys Lett* 1991;58:2435–7. doi:10.1063/1.104865.
- [33] Zhang L, Xue D. Preparation and magnetic properties of pure CoO nanoparticles. *J Mater Sci Lett* 2002;21:1931–3. doi:10.1023/A:1021656529934.
- [34] Chen D-H, Wu S-H. Synthesis of Nickel Nanoparticles in Water-in-Oil Microemulsions. *Chem Mater* 2000;12:1354–60. doi:10.1021/cm991167y.
- [35] Oguri Y, Riman RE, Bowen HK. Processing of anatase prepared from hydrothermally treated alkoxy-derived hydrous titania. *J Mater Sci* 1988;23:2897–904. doi:10.1007/BF00547465.
- [36] Cheng H, Ma J, Zhao Z, Qi L. Hydrothermal Preparation of Uniform Nanosize Rutile and Anatase Particles. *Chem Mater* 1995;7:663–71. doi:10.1021/cm00052a010.
- [37] Komarneni S, Roy R, Li QH. Microwave-hydrothermal synthesis of ceramic powders. *Mater Res Bull* 1992;27:1393–405. doi:10.1016/0025-5408(92)90004-J.
- [38] Meldrum FC, Wade VJ, Nimmo DL, Heywood BR, Mann S. Synthesis of Inorganic Nanophase Materials in Supramolecular Protein Cages. *Nature* 1991;349:684–7. doi:10.1038/349684a0.
- [39] Douglas T, Strable E, Willits D, Aitouchen A, Libera M, Young M. Protein Engineering of a Viral Cage for Constrained Nanomaterials Synthesis. *Adv Mater* 2002;14:415–8. doi:10.1002/1521-4095(20020318)14:6<415::AID-ADMA415>3.0.CO;2-W.
- [40] Phuoc TX, Soong Y, Chyu MK. Synthesis of Ag-deionized water nanofluids using multi-beam laser ablation in liquids. *Opt Lasers Eng* 2007;45:1099–106.
- [41] Han ZH, Cao FY, Yang B. Synthesis and thermal characterization of phase-changeable indium/polyalphaolefin nanofluids. *Appl Phys Lett* 2008;92:243104.
- [42] Tavares J, Coulombe S. Dual plasma synthesis and characterization of a stable copper-ethylene glycol nanofluid. *Powder Technol* 2011;210:132–42.
- [43] Hauser EA. The history of colloid science: In memory of Wolfgang Ostwald. *J Chem Educ* 1955;32:2. doi:10.1021/ed032p2.
- [44] Ghadimi A, Saidur R, Metselaar HSC. A review of nanofluid stability properties and characterization in stationary conditions. *Int J Heat Mass Transf* 2011;54:4051–68.

- [45] Bergman TL. Effect of reduced specific heats of nanofluids on single phase, laminar internal forced convection. *Int J Heat Mass Transf* 2009;52:1240–4.
- [46] Özerinç S, Kakaç S, Yazıcıoğlu AG. Enhanced thermal conductivity of nanofluids: a state-of-the-art review. *Microfluid Nanofluidics* 2010;8:145–70. doi:10.1007/s10404-009-0524-4.
- [47] Liu Y-D, Zhou Y-G, Tong M-W, Zhou X-S. Experimental study of thermal conductivity and phase change performance of nanofluids PCMs. *Microfluid Nanofluidics* 2009;7:579–84.
- [48] Kang HU, Kim SH, Oh JM. Estimation of thermal conductivity of nanofluid using experimental effective particle volume. *Exp Heat Transf* 2006;19:181–91.
- [49] Keblinski P, Prasher R, Eapen J. Thermal conductance of nanofluids: is the controversy over? *J Nanoparticle Res* 2008;10:1089–97.
- [50] Hwang Y, Lee JK, Lee CH, Jung YM, Cheong SI, Lee CG, et al. Stability and thermal conductivity characteristics of nanofluids. *Thermochim Acta* 2007;455:70–4.
- [51] Murshed SMS, Leong KC, Yang C. Investigations of thermal conductivity and viscosity of nanofluids. *Int J Therm Sci* 2008;47:560–8.
- [52] Yoo D-H, Hong KS, Yang H-S. Study of thermal conductivity of nanofluids for the application of heat transfer fluids. *Thermochim Acta* 2007;455:66–9. doi:<http://dx.doi.org/10.1016/j.tca.2006.12.006>.
- [53] Liu M-S, Lin MC-C, Tsai CY, Wang C-C. Enhancement of thermal conductivity with Cu for nanofluids using chemical reduction method. *Int J Heat Mass Transf* 2006;49:3028–33.
- [54] Hwang YJ, Ahn YC, Shin HS, Lee CG, Kim GT, Park HS, et al. Investigation on characteristics of thermal conductivity enhancement of nanofluids. *Curr Appl Phys* 2006;6:1068–71.
- [55] Zhang X, Gu H, Fujii M. Effective thermal conductivity and thermal diffusivity of nanofluids containing spherical and cylindrical nanoparticles. *Exp Therm Fluid Sci* 2007;31:593–9. doi:<http://dx.doi.org/10.1016/j.expthermflusci.2006.06.009>.
- [56] Hwang Y, Park HS, Lee JK, Jung WH. Thermal conductivity and lubrication characteristics of nanofluids. *Curr Appl Phys* 2006;6:e67–71.
- [57] Zhang X, Gu H, Fujii M. Experimental study on the effective thermal conductivity and thermal diffusivity of nanofluids. *Int J Thermophys* 2006;27:569–80.
- [58] Kwak K, Kim C. Viscosity and thermal conductivity of copper oxide nanofluid dispersed in ethylene glycol. *Korea-Australia Rheol J* 2005;17:35–40.
- [59] Evans W, Prasher R, Fish J, Meakin P, Phelan P, Keblinski P. Effect of aggregation and

- interfacial thermal resistance on thermal conductivity of nanocomposites and colloidal nanofluids. *Int J Heat Mass Transf* 2008;51:1431–8.
- [60] Putra N, Thiesen P, Roetzel W. Temperature dependence of thermal conductivity enhancement for nanofluids. *J Heat Transf* 2003;125:567–74.
- [61] Pastoriza-Gallego MJ, Lugo L, Legido JL, Piñeiro MM. Thermal conductivity and viscosity measurements of ethylene glycol-based Al₂O₃ nanofluids. *Nanoscale Res Lett* 2011;6:1–11.
- [62] White SB, Shih AJ-M, Pipe KP. Investigation of the electrical conductivity of propylene glycol-based ZnO nanofluids. *Nanoscale Res Lett* 2011;6:346. doi:10.1186/1556-276X-6-346.
- [63] Mintsa HA, Roy G, Nguyen CT, Doucet D. New temperature dependent thermal conductivity data for water-based nanofluids. *Int J Therm Sci* 2009;48:363–71.
- [64] Kim SH, Choi SR, Kim D. Thermal conductivity of metal-oxide nanofluids: particle size dependence and effect of laser irradiation. *J Heat Transfer* 2007;129:298–307.
- [65] Wang X, Li X, Yang S. Influence of pH and SDBS on the stability and thermal conductivity of nanofluids. *Energy & Fuels* 2009;23:2684–9.
- [66] Vajjha RS, Das DK. Experimental determination of thermal conductivity of three nanofluids and development of new correlations. *Int J Heat Mass Transf* 2009;52:4675–82.
- [67] Hong T-K, Yang H-S, Choi CJ. Study of the enhanced thermal conductivity of Fe nanofluids. *J Appl Phys* 2005;97:64311.
- [68] Kleinstreuer C, Feng Y. Experimental and theoretical studies of nanofluid thermal conductivity enhancement: a review. *Nanoscale Res Lett* 2011;6:1–13.
- [69] Timofeeva E V, Gavrilov AN, McCloskey JM, Tolmachev Y V, Sprunt S, Lopatina LM, et al. Thermal conductivity and particle agglomeration in alumina nanofluids: experiment and theory. *Phys Rev E* 2007;76:61203.
- [70] Hong KS, Hong T-K, Yang H-S. Thermal conductivity of Fe nanofluids depending on the cluster size of nanoparticles. *Appl Phys Lett* 2006;88:31901.
- [71] Yu W, Xie H, Chen L, Li Y. Investigation of thermal conductivity and viscosity of ethylene glycol based ZnO nanofluid. *Thermochim Acta* 2009;491:92–6.
- [72] Patel HE, Das SK, Sundararajan T, Sreekumaran Nair A, George B, Pradeep T. Thermal conductivities of naked and monolayer protected metal nanoparticle based nanofluids: Manifestation of anomalous enhancement and chemical effects. *Appl Phys Lett* 2003;83:2931–3.
- [73] Yu W, France DM, Routbort JL, Choi SUS. Review and comparison of nanofluid thermal

- conductivity and heat transfer enhancements. *Heat Transf Eng* 2008;29:432–60.
- [74] Eastman JA, Choi SUS, Li S, Yu W, Thompson LJ. Anomalous increased effective thermal conductivities of ethylene glycol-based nanofluids containing copper nanoparticles. *Appl Phys Lett* 2001;78:718–20.
- [75] Lee J-H, Hwang KS, Jang SP, Lee BH, Kim JH, Choi SUS, et al. Effective viscosities and thermal conductivities of aqueous nanofluids containing low volume concentrations of Al₂O₃ nanoparticles. *Int J Heat Mass Transf* 2008;51:2651–6.
- [76] Zhu H, Zhang C, Liu S, Tang Y, Yin Y. Effects of nanoparticle clustering and alignment on thermal conductivities of Fe₃O₄ aqueous nanofluids. *Appl Phys Lett* 2006;89:23123.
- [77] Murshed SMS, Leong KC, Yang C. A combined model for the effective thermal conductivity of nanofluids. *Appl Therm Eng* 2009;29:2477–83.
- [78] Yang B, Han ZH. Temperature-dependent thermal conductivity of nanorod-based nanofluids. *Appl Phys Lett* 2006;89:83111.
- [79] Buongiorno J, Venerus DC, Prabhat N, McKrell T, Townsend J, Christianson R, et al. A benchmark study on the thermal conductivity of nanofluids. *J Appl Phys* 2009;106:94312.
- [80] Xie H, Lee H, Youn W, Choi M. Nanofluids containing multiwalled carbon nanotubes and their enhanced thermal conductivities. *J Appl Phys* 2003;94:4967–71.
- [81] Prasher R, Evans W, Meakin P, Fish J, Phelan P, Keblinski P. Effect of aggregation on thermal conduction in colloidal nanofluids. *Appl Phys Lett* 2006;89:143119.
- [82] Jang SP, Choi SUS. Role of Brownian motion in the enhanced thermal conductivity of nanofluids. *Appl Phys Lett* 2004;84:4316–8.
- [83] Li CH, Peterson GP. The effect of particle size on the effective thermal conductivity of Al₂O₃-water nanofluids. *J Appl Phys* 2007;101:44312.
- [84] Eapen J, Williams WC, Buongiorno J, Hu L, Yip S, Rusconi R, et al. Mean-field versus microconvection effects in nanofluid thermal conduction. *Phys Rev Lett* 2007;99:95901.
- [85] Wensel J, Wright B, Thomas D, Douglas W, Mannhalter B, Cross W, et al. Enhanced thermal conductivity by aggregation in heat transfer nanofluids containing metal oxide nanoparticles and carbon nanotubes. *Appl Phys Lett* 2008;92:23110.
- [86] Wright B, Thomas D, Hong H, Groven L, Puszynski J, Duke E, et al. Magnetic field enhanced thermal conductivity in heat transfer nanofluids containing Ni coated single wall carbon nanotubes. *Appl Phys Lett* 2007;91:173116.
- [87] Vollath D. Plasma synthesis of nanopowders. *J Nanoparticle Res* 2008;10:39.
- [88] Botha SS. Synthesis and characterization of nanofluids for cooling applications 2006.
- [89] Chen X, Mao SS. Titanium dioxide nanomaterials: synthesis, properties, modifications,

- and applications. *Chem Rev* 2007;107:2891–959.
- [90] Lo C-H, Tsung T-T, Lin H-M. Preparation of silver nanofluid by the submerged arc nanoparticle synthesis system (SANSS). *J Alloys Compd* 2007;434:659–62.
- [91] Kumar DH, Patel HE, Kumar VRR, Sundararajan T, Pradeep T, Das SK. Model for heat conduction in nanofluids. *Phys Rev Lett* 2004;93:144301.
- [92] Prasher R, Bhattacharya P, Phelan PE. Thermal conductivity of nanoscale colloidal solutions (nanofluids). *Phys Rev Lett* 2005;94:25901.
- [93] Lee J, Gharagozloo PE, Kolade B, Eaton JK, Goodson KE. Nanofluid convection in microtubes. *J Heat Transfer* 2010;132:92401.
- [94] Lai WY, Vinod S, Phelan PE, Prasher R. Convective heat transfer for water-based alumina nanofluids in a single 1.02-mm tube. *J Heat Transfer* 2009;131:112401.
- [95] Heris SZ, Etemad SG, Esfahany MN. Experimental investigation of oxide nanofluids laminar flow convective heat transfer. *Int Commun Heat Mass Transf* 2006;33:529–35.
- [96] Wen D, Ding Y. Experimental investigation into convective heat transfer of nanofluids at the entrance region under laminar flow conditions. *Int J Heat Mass Transf* 2004;47:5181–8.
- [97] Heris SZ, Esfahany MN, Etemad SG. Experimental investigation of convective heat transfer of Al₂O₃/water nanofluid in circular tube. *Int J Heat Fluid Flow* 2007;28:203–10.
- [98] Williams W, Buongiorno J, Hu L-W. Experimental investigation of turbulent convective heat transfer and pressure loss of alumina/water and zirconia/water nanoparticle colloids (nanofluids) in horizontal tubes. *J Heat Transfer* 2008;130:42412.
- [99] Daungthongsuk W, Wongwises S. A critical review of convective heat transfer of nanofluids. *Renew Sustain Energy Rev* 2007;11:797–817.
- [100] Jung J-Y, Oh H-S, Kwak H-Y. Forced convective heat transfer of nanofluids in microchannels. *Int J Heat Mass Transf* 2009;52:466–72.
- [101] Buongiorno J. Convective transport in nanofluids. *J Heat Transfer* 2006;128:240–50.
- [102] S. U. S. Choi and J. A. Eastman. Enhancing Thermal Conductivity of Fluids With Nanoparticles. *Am. Soc. Mech. Eng.*, 1995, p. 99–105.
- [103] Kisielowski C, Freitag B, Bischoff M, van Lin H, Lazar S, Knippels G, et al. Detection of Single Atoms and Buried Defects in Three Dimensions by Aberration-Corrected Electron Microscope with 0.5-Å Information Limit. *Microsc Microanal* 2008;14:469–77. doi:10.1017/S1431927608080902.
- [104] Sawada H, Hosokawa F, Kaneyama T, Ishizawa T, Terao M, Kawazoe M, et al. Achieving 63 pm Resolution in Scanning Transmission Electron Microscope with Spherical Aberration Corrector. *Jpn J Appl Phys* 2007;46:L568.

- [105] Pennycook, Rafferty, Nellist. Z-contrast Imaging in an Aberration-corrected Scanning Transmission Electron Microscope. *Microsc Microanal* 2000;6:343–52. doi:10.1017.S1431927600000532.
- [106] Sohlberg K, Rashkeev S, Borisevich AY, Pennycook SJ, Pantelides ST. Origin of Anomalous Pt-Pt Distances in the Pt/Alumina Catalytic System. *ChemPhysChem* 2004;5:1893–7. doi:10.1002/cphc.200400212.
- [107] Qiao B, Wang A, Yang X, Allard LF, Jiang Z, Cui Y, et al. Single-atom catalysis of CO oxidation using Pt1/FeOx. *Nat Chem* 2011;3:634–41.
- [108] Lin J, Qiao B, Liu J, Huang Y, Wang A, Li L, et al. Design of a Highly Active Ir/Fe(OH)_x Catalyst: Versatile Application of Pt-Group Metals for the Preferential Oxidation of Carbon Monoxide. *Angew Chemie Int Ed* 2012;51:2920–4. doi:10.1002/anie.201106702.
- [109] Zhou W, Ross-Medgaarden EI, Knowles W V, Wong MS, Wachs IE, Kiely CJ. Identification of active Zr–WO_x clusters on a ZrO₂ support for solid acid catalysts. *Nat Chem* 2009;1:722–8.
- [110] Herzing AA, Kiely CJ, Carley AF, Landon P, Hutchings GJ. Identification of Active Gold Nanoclusters on Iron Oxide Supports for CO Oxidation. *Science (80-)* 2008;321:1331 LP-1335.
- [111] Su DS, Jacob T, Hansen TW, Wang D, Schlögl R, Freitag B, et al. Surface Chemistry of Ag Particles: Identification of Oxide Species by Aberration-Corrected TEM and by DFT Calculations. *Angew Chemie Int Ed* 2008;47:5005–8. doi:10.1002/anie.200800406.
- [112] Gontard LC, Chang L-Y, Hetherington CJD, Kirkland AI, Ozkaya D, Dunin-Borkowski RE. Aberration-Corrected Imaging of Active Sites on Industrial Catalyst Nanoparticles. *Angew Chemie Int Ed* 2007;46:3683–5. doi:10.1002/anie.200604811.
- [113] Akita T, Kohyama M, Haruta M. Electron Microscopy Study of Gold Nanoparticles Deposited on Transition Metal Oxides. *Acc Chem Res* 2013;46:1773–82. doi:10.1021/ar300259n.
- [114] Su DS. Special Issue: Advanced Electron Microscopy for Catalysis. *ChemCatChem* 2011;3:919–20. doi:10.1002/cctc.201100175.
- [115] Sohlberg K, Pennycook TJ, Zhou W, Pennycook SJ. Insights into the physical chemistry of materials from advances in HAADF-STEM. *Phys Chem Chem Phys* 2015;17:3982–4006. doi:10.1039/C4CP04232H.
- [116] Takeda S, Yoshida H. Atomic-resolution environmental TEM for quantitative in-situ microscopy in materials science. *Microscopy* 2013;62:193–203.
- [117] Leary R, Midgley PA, Thomas JM. Recent Advances in the Application of Electron Tomography to Materials Chemistry. *Acc Chem Res* 2012;45:1782–91. doi:10.1021/ar3001102.

- [118] Friedrich H, de Jongh PE, Verkleij AJ, de Jong KP. Electron Tomography for Heterogeneous Catalysts and Related Nanostructured Materials. *Chem Rev* 2009;109:1613–29. doi:10.1021/cr800434t.
- [119] Liu J. Advanced Electron Microscopy Characterization of Nanostructured Heterogeneous Catalysts. *Microsc Microanal* 2004;10:55–76. doi:10.1017/S1431927604040310.
- [120] Liu JJ. Advanced Electron Microscopy of Metal-Support Interactions in Supported Metal Catalysts. *ChemCatChem* 2011;3:934–48. doi:10.1002/cctc.201100090.
- [121] Zhang S, Nguyen L, Zhu Y, Zhan S, Tsung C-K (Frank), Tao F (Feng). In-Situ Studies of Nanocatalysis. *Acc Chem Res* 2013;46:1731–9. doi:10.1021/ar300245g.
- [122] Grunwaldt J-D, Wagner JB, Dunin-Borkowski RE. Imaging Catalysts at Work: A Hierarchical Approach from the Macro- to the Meso- and Nano-scale. *ChemCatChem* 2013;5:62–80. doi:10.1002/cctc.201200356.
- [123] Thomas JM, Leary R, Midgley PA, Holland DJ. A new approach to the investigation of nanoparticles: Electron tomography with compressed sensing. *J Colloid Interface Sci* 2013;392:7–14. doi:https://doi.org/10.1016/j.jcis.2012.09.068.
- [124] Bernal S, Baker RT, Burrows A, Calvino JJ, Kiely CJ, López-Cartes C, et al. Structure of highly dispersed metals and oxides: exploring the capabilities of high-resolution electron microscopy. *Surf Interface Anal* 2000;29:411–21. doi:10.1002/1096-9918(200007)29:7<411::AID-SIA824>3.0.CO;2-F.
- [125] Thomas JM, Terasaki O, Gai PL, Zhou W, Gonzalez-Calbet J. Structural Elucidation of Microporous and Mesoporous Catalysts and Molecular Sieves by High-Resolution Electron Microscopy. *Acc Chem Res* 2001;34:583–94. doi:10.1021/ar970352j.
- [126] Gai PL. Developments of electron microscopy methods in the study of catalysts. *Curr Opin Solid State Mater Sci* 2001;5:371–80. doi:https://doi.org/10.1016/S1359-0286(01)00036-5.
- [127] Datye AK, Xu Q, Kharas KC, McCarty JM. Particle size distributions in heterogeneous catalysts: What do they tell us about the sintering mechanism? *Catal Today* 2006;111:59–67. doi:https://doi.org/10.1016/j.cattod.2005.10.013.
- [128] Wang D, Villa A, Su D, Prati L, Schlögl R. Carbon-Supported Gold Nanocatalysts: Shape Effect in the Selective Glycerol Oxidation. *ChemCatChem* 2013;5:2717–23. doi:10.1002/cctc.201200535.
- [129] Gan L, Rudi S, Cui C, Strasser P. Ni-Catalyzed Growth of Graphene Layers during Thermal Annealing: Implications for the Synthesis of Carbon-Supported PtNi Fuel-Cell Catalysts. *ChemCatChem* 2013;5:2691–4. doi:10.1002/cctc.201300235.
- [130] Zhang W, Chen M, Theil Kuhn L, Bowen JR, Bentzen JJ. Electrochemistry Unlocks Wettability: Epitaxial Growth of Oxide Nanoparticles on Rough Metallic Surfaces. *ChemElectroChem* 2014;1:520–3. doi:10.1002/celec.201300045.

- [131] Chen X-W, Su DS, Hamid SBA, Schlögl R. The morphology, porosity and productivity control of carbon nanofibers or nanotubes on modified activated carbon. *Carbon N Y* 2007;45:895–8. doi:<https://doi.org/10.1016/j.carbon.2006.12.005>.
- [132] Muller J-O, Su DS, Wild U, Schlogl R. Bulk and surface structural investigations of diesel engine soot and carbon black. *Phys Chem Chem Phys* 2007;9:4018–25. doi:10.1039/B704850E.
- [133] Su DS, Zhu ZP, Liu X, Weinberg G, Wang N, Schlögl R, et al. Assembly of carbon tube-in-tube nanostructures. *AIP Conf Proc* 2005;786:296–300. doi:10.1063/1.2103873.
- [134] Marks LD. Experimental studies of small particle structures. *Reports Prog Phys* 1994;57:603.
- [135] Smith DJ. The realization of atomic resolution with the electron microscope. *Reports Prog Phys* 1997;60:1513.
- [136] Yacamán MJ, Heinemann K, Poppa H. The determination of the habit planes of nanometer-size single-crystal gold particles. *Crit Rev Solid State Mater Sci* 1981;10:243–60. doi:10.1080/10408438108243636.
- [137] Marks LD. Inhomogeneous strains in small particles. *Surf Sci* 1985;150:302–18. doi:[http://dx.doi.org/10.1016/0039-6028\(85\)90648-X](http://dx.doi.org/10.1016/0039-6028(85)90648-X).
- [138] Lin J, Wang A, Qiao B, Liu X, Yang X, Wang X, et al. Remarkable Performance of Ir1/FeOx Single-Atom Catalyst in Water Gas Shift Reaction. *J Am Chem Soc* 2013;135:15314–7. doi:10.1021/ja408574m.
- [139] Genc A, Kovarik L, Gu M, Cheng H, Plachinda P, Pullan L, et al. XEDS STEM tomography for 3D chemical characterization of nanoscale particles. *Ultramicroscopy* 2013;131:24–32. doi:<https://doi.org/10.1016/j.ultramic.2013.03.023>.
- [140] DE ROSIER DJ, KLUG A. Reconstruction of Three Dimensional Structures from Electron Micrographs. *Nature* 1968;217:130–4.
- [141] Hart RG. Electron Microscopy of Unstained Biological Material: The Polytopic Montage. *Science (80-)* 1968;159:1464 LP-1467.
- [142] Meyer JC, Chuvilin A, Algara-Siller G, Biskupek J, Kaiser U. Selective Sputtering and Atomic Resolution Imaging of Atomically Thin Boron Nitride Membranes. *Nano Lett* 2009;9:2683–9. doi:10.1021/nl9011497.
- [143] Egerton RF. Control of radiation damage in the TEM. *Ultramicroscopy* 2013;127:100–8. doi:10.1016/j.ultramic.2012.07.006.
- [144] Zobelli A, Gloter A, Ewels CP, Seifert G, Colliex C. Electron knock-on cross section of carbon and boron nitride nanotubes. *Phys Rev B* 2007;75:245402. doi:10.1103/PhysRevB.75.245402.

- [145] Kaiser U, Biskupek J, Meyer JC, Leschner J, Lechner L, Rose H, et al. Transmission electron microscopy at 20 kV for imaging and spectroscopy. *Ultramicroscopy* 2011;111:1239–46. doi:10.1016/j.ultramic.2011.03.012.
- [146] Bell DC, Russo CJ, Kolmykov D V. 40 keV atomic resolution TEM. *Ultramicroscopy* 2012;114:31–7. doi:https://doi.org/10.1016/j.ultramic.2011.12.001.
- [147] Drummy LF, Yang J, Martin DC. Low-voltage electron microscopy of polymer and organic molecular thin films. *Ultramicroscopy* 2004;99:247–56. doi:10.1016/j.ultramic.2004.01.011.
- [148] Yang X-F, Wang A, Qiao B, Li J, Liu J, Zhang T. Single-Atom Catalysts: A New Frontier in Heterogeneous Catalysis. *Acc Chem Res* 2013;46:1740–8. doi:10.1021/ar300361m.
- [149] Uzun A, Ortalan V, Browning ND, Gates BC. Site-isolated iridium complexes on MgO powder: individual Ir atoms imaged by scanning transmission electron microscopy. *Chem Commun (Camb)* 2009:4657–9. doi:10.1039/b823171k.
- [150] He S, Li C, Chen H, Su D, Zhang B, Cao X, et al. A Surface Defect-Promoted Ni Nanocatalyst with Simultaneously Enhanced Activity and Stability. *Chem Mater* 2013;25:1040–6. doi:10.1021/cm303517z.
- [151] IJJIMA S. Electron Microscopy of Small Particles. *J Electron Microsc (Tokyo)* 1985;34:249–65.
- [152] Li L, Zhang B, Kunkes E, Föttinger K, Armbrüster M, Su DS, et al. Ga-Pd/Ga₂O₃ Catalysts: The Role of Gallia Polymorphs, Intermetallic Compounds, and Pretreatment Conditions on Selectivity and Stability in Different Reactions. *ChemCatChem* 2012;4:1764–75. doi:10.1002/cctc.201200268.
- [153] Ino S, Ogawa S. Multiply Twinned Particles at Earlier Stages of Gold Film Formation on Alkali halide Crystals. *J Phys Soc Japan* 1967;22:1365–74. doi:10.1143/JPSJ.22.1365.
- [154] Jefferson DA, Thomas JM, Millward GR, Tsuno K, Harriman A, Brydson RD. Atomic structure of ultrafine catalyst particles resolved with a 200-keV transmission electron microscope. *Nature* 1986;323:428–31.
- [155] Urban J, Sack-Kongehl H, Weiss K. Computer simulations of HREM images of metal clusters. *Zeitschrift Für Phys D Atoms, Mol Clust* 1993;28:247–55. doi:10.1007/BF01437891.
- [156] Bernal S, Botana FJ, Calvino JJ, López-Cartes C, Pérez-Omil JA, Rodríguez-Izquierdo JM. The interpretation of HREM images of supported metal catalysts using image simulation: profile view images. *Ultramicroscopy* 1998;72:135–64. doi:https://doi.org/10.1016/S0304-3991(98)00009-6.
- [157] Pan X, Zhang B, Zhong B, Wang J, Su DS. Towards a highly dispersed and more thermally stable Ru/OCNT catalyst. *Chem Commun* 2014;50:3856–8. doi:10.1039/C3CC48710E.

- [158] Zhang Z, Su D. Behaviour of TEM metal grids during in-situ heating experiments. *Ultramicroscopy* 2009;109:766–74. doi:<https://doi.org/10.1016/j.ultramic.2009.01.015>.
- [159] Kumar SS, Venkateswarlu P, Rao VR, Rao GN. Synthesis , characterization and optical properties of zinc oxide nanoparticles. *Int Nano Lett* 2013:1–6.
- [160] Marcano A, Cabrera H, Guerra M, Cruz R a., Jacinto C, Catunda T. Optimizing and calibrating a mode-mismatched thermal lens experiment for low absorption measurement. *J Opt Soc Am B* 2006;23:1408. doi:10.1364/JOSAB.23.001408.
- [161] Cruz RA, Jacinto C, Catunda T, Física I De, Carlos DS, Paulo UDS, et al. High-Sensitivity Absorption Measurements in Liquids and Solids 2006:2–5.
- [162] Marcano A, Loper C, Melikechi N. No Title Pump-probe mode mismatched Z scan. *J Opt Soc* 2002;19:119–24.
- [163] Yıldırım ÖA, Durucan C. Effect of precipitation temperature and organic additives on size and morphology of ZnO nanoparticles. *J Mater Res* 2012;27:1452–61. doi:10.1557/jmr.2012.58.
- [164] Kooti M, Sedeh AN. Microwave-Assisted Combustion Synthesis of ZnO Nanoparticles. *J Chem* 2013;2013.
- [165] Barreto G, Morales G, Cañizo A, Eyler N. Microwave assisted synthesis of ZnO tridimensional nanostructures. *Procedia Mater Sci* 2015;8:535–40. doi:10.1016/j.mspro.2015.04.106.
- [166] Hasanpoor M, Aliofkhaezrai M, Delavari H. Microwave-assisted synthesis of zinc oxide nanoparticles. *Procedia Mater Sci* 2015;11:320–5. doi:10.1016/j.mspro.2015.11.101.
- [167] Wang W, Zhu Y. Shape-controlled synthesis of zinc oxide by microwave heating using an imidazolium salt. *Inorg Chem Commun* 2004;7:1003–5. doi:10.1016/j.inoche.2004.06.014.
- [168] Griffith M, Udekwu KI, Gkatzis S, Mah T, Alarcon EI. Synthetic Routes for the Preparation of Silver Nanoparticles A Mechanistic Perspective. *Silver Nanoparticle Appl.*, 2015, p. 127–46. doi:10.1007/978-3-319-11262-6.
- [169] Paramelle D, Sadovoy A, Gorelik S, Free P, Hopley J, Fernig DG. A rapid method to estimate the concentration of citrate capped silver nanoparticles from UV-visible light spectra. *Analyst* 2014;139:4855–61. doi:10.1039/c4an00978a.
- [170] Oldenburg S. nanoComposix, Precisely engineered, highly characterized 2017. <https://nanocomposix.com> (accessed June 23, 2017).

